J. Fluid Mech. (2013), *vol.* 731, *pp.* 223–258.
doi:10.1017/jfm.2013.232

Towards modular analysis of tropical-cyclone structure: the boundary layer

Francis Fendell[1],† **and Paritosh Mokhasi**[2]

[1]Northrop Grumman Aerospace Systems, Redondo Beach, CA 90278, USA
[2]Wolfram Research Inc., Champaign, IL 61820, USA

(Received 2 November 2011; revised 18 March 2013; accepted 2 May 2013;
first published online 14 August 2013)

In the early 1970s, George Carrier and coworkers undertook a modular approach to modelling the internal thermofluid-dynamics of tropical cyclones of tropical-depression-or-greater intensity. A novel, relatively simplistic, approximate analysis of the vortex, idealized as axisymmetric, was carried out in the asymptotic limit of large Reynolds number, so that inviscid and diffusive subdomains of the structure were distinguished. Little subsequent work has followed this line of investigation. The indifference has proven problematic because accurate prediction of tropical-cycling intensity remains a challenge for operational forecasting, despite decades of effort at direct integration of comprehensive boundary/initial-value formulations. A contributing factor is that, to achieve solution in real time, such computational treatment of the entire vortex invariably resorts to coarse gridding, and key features remain inadequately resolved. Accordingly, here the modular approach is revisited, with the assistance of: recent observational insights; greatly enhanced computer-processing power; and convenient computational software, which facilitates implementation of a semi-analytic, semi-numerical methodology. Focus is largely, but not exclusively, on the dynamics and energetics occurring in the nominally kilometre-thick, ocean-surface-contiguous boundary layer, especially on influx to the boundary layer and efflux therefrom. The modular approach not only permits the boundary layer, which develops its own highly significant substructure under the high-speed portion of the inviscid vortex, to be well-resolved, but also allows the layer to be investigated in the context of the other tropical-cyclone-structure subdivisions.

Key words: atmospheric flows, boundary layers, rotating flows

1. Introduction

Tropical cyclones are seasonally recurrent, high-impact natural hazards, arising episodically in almost all of the Earth's tropical-ocean basins (Musk 1988). Virtually any contemporary discussion of these relatively large-lateral-dimension, relatively long-lived, troposphere-filling vortices (e.g. Marks 2003) recounts that, over the past two decades, progress in individual global-scale-forecast models, in conjunction with the introduction of ensemble forecasts based on such models, has halved the typical

† Email address for correspondence: frank.fendell@ngc.com

error in track prediction. Today, the characteristic error in path prognostication in the North Atlantic and eastern North Pacific basins increases by roughly 90 km for every 24 h into the future, up to five days (Rappaport & Franklin 2008). The same discussion acknowledges that only miniscule assistance to upgrade tropical-cyclone-intensity forecasts has been derived from investigations pursued during those two decades (see also Baum & Fendell 2006*a*,*b*). Intensity is characterized traditionally by the peak low-altitude sustained wind speed occurring within the vortex. Nominally, in the US, the reference is to one-minute-averaged wind at 10 m altitude above sea level, but this traditional definition is not followed uniformly in practice, e.g. because of wave height. Observationally, a particular sea-level pressure anomaly (deficit) at the vortex centre relative to the vortex periphery cannot be associated uniquely with a particular wind-based intensity, so both pressure anomaly and peak sustained swirl are included in typical intensity forecasts and archival data (Beven II & Lixion 2008).

Whereas the track of a tropical cyclone is predominantly a consequence of ambient winds and pressure, intensity is predominantly a consequence of the thermofluid-dynamics holding within the vortex proper. Since it may be many decades before American global-forecast systems, which currently utilize a 25 km-or-coarser lateral grid, achieve the at least one-kilometre resolution requisite to describe the crucial core of a tropical cyclone (Baum & Fendell 2006*a*,*b*), the prevailing approach to elucidate the internal processes is via direct detailed numerical simulation with a local-area model, proceeding from the fundamental conservation laws and boundary/initial conditions. However, the broad, multiscale range of pertinent physical processes within a vortex of ∼700–1000 km diameter necessitates the parameterization of the accumulative contribution of such typically subgrid-scale processes as cumulus convection, cloud microphysics, turbulent mixing, radiative transfer, and air–sea interaction. The common response of contemporary modellers to shortfalls in intensity forecasts is adoption of ever-more-detailed, ever-more-computationally demanding, but still speculative and possibly error-prone parameterizations. A consequence is adoption of coarse computational grids to achieve even a single solution in real time, let alone ensembles. Large gradients in some subdomains of the tropical-cyclone structure are smeared out, to the detriment of the computational effort. For example, in effect, the description is hydrostatic at sites at which nonlinear convective transport might be expected to contribute significantly.

These contemporary issues regarding tradeoffs in formulation of tropical-cyclone models were foreshadowed decades ago. At that time, George Carrier and his colleagues (Carrier, Hammond & George 1971; Carrier 1971*a*,*b*; Fendell 1974) suggested that the major impediment to upgraded intensity forecasts lay in incomplete knowledge and misconceptions regarding the macroscale thermofluid-dynamics, rather than in shortcoming in the inclusiveness of parameterizations.

1.1. *Modular analysis*

Carrier undertook an approximate, highly resolved, yet tractable treatment of modules comprising the tropical-cyclone structure by retaining only the locally dominant processes, and exploiting the locally dominant gradients, in each mathematically and physically distinct subdomain. He then sought to fuse the local solutions into a global, uniformly valid composite by enforcing appropriate conditions of continuity at the interfaces, or strips of overlapping validity, between neighbouring subdomains (figures 1 and 2). Such an approach has been beneficially adopted in myriad applications in all branches of continuum mechanics over the last century (e.g. Cole 1968), either with formality (singular perturbation) or heuristically (boundary-layer

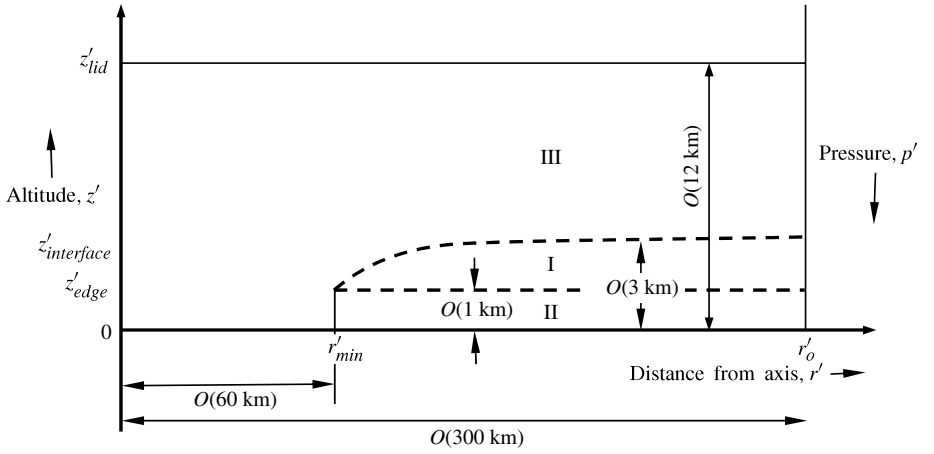

FIGURE 1. Schematic, not to scale, of a steady axisymmetric tropical cyclone of tropical-depression or tropical-storm intensity, of given radial extent r'_o and inferred vertical extent z'_{lid}. The model with an open boundary at r'_o consists of three modules: the bulk vortex, I; the constant-thickness boundary layer, II; and the core (which evolves into an upper-tropospheric outflow), III. The position and properties of the interface (between modules I and III), which extends from (r'_{min}, z'_{edge}), to $(r'_o, z'_{interface})$, are to be found in the course of solution.

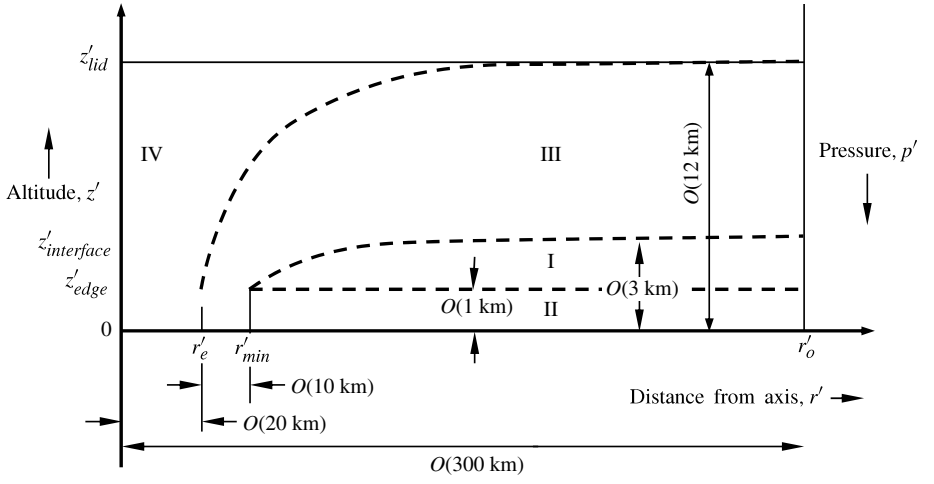

FIGURE 2. Schematic, not to scale, of a steady axisymmetric tropical cyclone of hurricane intensity. The radius of boundary-layer separation r'_{min} is smaller than in figure 1, and the core III is confined to an annulus, owing to the presence of an additional, central module IV, the eye. The position and properties of the interface between modules III and IV, and between modules I and III, are to be found in the course of solution. Since here the eye descends to sea level $z' = 0$, the schematic typifies a major hurricane.

theory). However, Carrier's introduction of the methodology in the asymptotic limit of large Reynolds number (or its rotating-flow counterpart, small Ekman number) appeared unconventional to most of the tropical-cyclone-modelling community, and was not carried further. Since the need for upgrade in tropical-cyclone-intensity

forecasting persists, and the modular approach remains largely unexplored by that community, we here re-examine the modular approach, and add to the results obtained with it.

2. A steady axisymmetric model of a mature tropical cyclone

2.1. *Classification*

Carrier does not address tropical disturbances, but instead initiates his modelling by postulating a three-module structure for a tropical depression (TD) or tropical storm (TS), idealized as quasi-steady and axisymmetric. The conventional threshold demarcating a TS (by definition, sustained swirl >17 m s^{-1}) from a less intense TD is regarded as an arbitrary distinction, even if widely cited and practically helpful. The three modules are (see figure 1): a bulk vortex (I) of swirling warm moist convectively unstable air, drawn from the lower troposphere of the autumnal maritime tropics, and serving as a supply of throughput, to be processed and then discharged back to the ambient at upper-tropospheric altitudes; a near-ocean-surface frictional boundary layer (II), fed over a large area by a modest net downdrift from (I), and conveying throughput radially inward under the action of a radial pressure gradient that persists across the layer (whereas the countervailing swirl-supported centrifugal 'force' is diffusively diminished across the layer, to comply with the no-slip constraint holding at the sea surface) (Turner 1966); and a boundary-layer-supplied, strongly convective, rapidly swirling, copiously precipitating core (III) that evolves to an upper-tropospheric outflow. Statistically (Diamond 2010), about half of TSs intensify further, to become hurricanes (Hs) (by definition, sustained swirl >33 m s^{-1}), in which case a fourth module, an eye (IV), complements the other three modules (see figure 2). The eye is a compressionally heated, slowly recirculating, virtually non-rotating, relatively dry, centrally situated module. Eye insertion confines the swirling updraft/outflow (III) to an annulus termed the eyewall (Carrier 1971*b*, figures 4 and 5). The conventional threshold demarcating a major hurricane (MH) (by definition, sustained swirl >50 m s^{-1}) from a less intense hurricane (H) is also an arbitrary distinction, but again, widely cited and practically helpful. Statistically (Diamond 2010), roughly about half of Hs intensify further to become MHs, the transition typically involving the eye drying out, extending further seaward, and becoming more radially confined.

A good summary of available monitoring data, which are consistent with the modular structure just outlined, is furnished by Marks (2003, pp. 949–957).

Seeking to identify observables for a one-in-two discrimination seems a more viable goal than seeking to identify observables for a one-in-ten discrimination of a future hurricane among nascent tropical disturbances.

2.2. *Open versus closed domains*

Carrier *et al.* (1971) adopted for their local-area model a closed domain, a uniformly rotating container of right-circular-cylinder configuration. The boundaries of the domain are: the nominally horizontal air–sea interface; the axis of symmetry; a horizontal conceptual lid at tropopause altitude (taken as the height at which sea-level moist air, vertically displaced to its lifting condensation level and thereafter spontaneously ascending on a moist-adiabatic locus of thermodynamic states (Houghton 1986), no longer has a density discrepancy relative to ambient air at the same altitude) (Palmèn & Newton 1969); and a conceptual cylindrical surface at the periphery. There may be diffusive, but not convective, transport across the boundaries.

More explicitly, the air–sea interface is taken as isothermal, the role of cooling of the sea surface by the inducing of a central, convective circulation, and of turbulent churning, within the underlying ocean (Gill 1982) being neglected. A small amount of slip may be admitted at the air–sea diffusive interface, but there seems no reason to express this slip in terms of a surface-drag coefficient (Taylor 2003), because so doing at high wind speed would amount to the arid formality of relating one unknown input quantity to another still uncertain quantity. Thermo-hydrostatically, the lid is taken to be slippery, isothermal, and isobaric. The cylindrical surface at the periphery is effectively non-slip.

The consequences of such a closed model include a quasi-steady once-through processing, in a finite-lifespan vortex, of a finite 'fuel supply' of convectively unstable air drawn from the autumnal maritime tropical ambient. Under the vortex, sea–air transfer of sensible and latent heat at approximately ambient levels persists. This transfer suffices to compensate for rainout, wherever and whenever the convective instability results, locally and transiently, in cumulus convection outside the core. So the convective instability is soon restored in module I, and persists on the temporal and spatial scales of interest to Carrier's investigation. Also, later-processed, originally midtropospheric air, during downdrift, approaches the total-static-enthalpy content of earlier-processed, originally lower-tropospheric air. Thus, for a while, the vortex is effectively self-sustaining. However, relatively dry, processed air is piled above a slowly depleted supply of relatively moist, still-to-be-processed air, and the vortex eventually decays, unless landfall intervenes sooner, in Carrier's depiction.

However, disadvantages of a closed model are as follows. There seems limited provision to incorporate the effect of a tropical cyclone eventually translating into an ambient environment with altered stratification. There seems limited provision to account for the upper-tropospheric outflow from the vortex. Also, physical mechanisms to maintain the convective instability of the 'captured' throughput that has yet to be processed need to be incorporated, and simulation of the intricate radiative–convective balance that sustains the stratification of the autumnal maritime tropical ambient is awkward for a simplistic model such as Carrier's, in which introduction of sophisticated parameterizations is avoided.

Here, a steady-state model with an open lateral boundary is examined. The particular convectively unstable stratification of the ambient environment under examination is a specified input, though the inflow rate across the periphery is internally controlled and subtle to infer. A self-consistent upper-tropospheric outflow from the vortex to the surrounding atmosphere is incorporated. No insight is provided into the rate of, or the intermediate states during, transition in response to altered ambient environments. The steady axisymmetric vortex being modelled has an annular, largely spiral-band-free bulk-vortex structure that is an uncommon but informative paradigm among tropical cyclones (Knaff, Kossin & DeMaria 2003).

2.3. *Some issues accentuated by a modular approach*

Some noteworthy properties of a mature tropical cyclone are accentuated by a modular approach, and are now discussed.

First, the tropical-cyclone boundary layer II (figure 1) is typically characterized as being between 0.5 and 2 km in thickness, with 1 km particularly frequently cited (Smith & Montgomery 2008; Smith & Vogl 2008). In general, until separation, the thickness of the boundary layer typically is characterized as not varying appreciably with increasing radial distance from the axis of rotation; the layer has been characterized to be of finite thickness at its lateral edge (Carrier *et al.* 1971 figure 1

and pp. 151–152). The pressure decreases roughly by about 100 hPa, by hydrostatic considerations, across a near-sea-level layer of 1 km thickness. Accordingly, the classical boundary-layer paradigm for a high-Reynolds-number scenario is modified whereby the inviscid-domain (I) solution is taken to hold only to a finite distance above the nominally planar sea-level altitude. The noteworthy thickness of the boundary layer is reflected in the adoption of an exceptionally large, empirically assigned eddy-diffusion coefficient, for a gradient-diffusion treatment of the turbulent transfer. Such a phenomenological treatment is adopted for its tractability; any enhanced vertical transfer due to special features, such as roll vortices, is incorporated by enhancing the eddy-diffusion coefficient.

Second, it is conventional in treating a large-Reynolds-number flow to pursue first the inviscid (bulk-vortex) solution, and then the boundary-layer solution to account for no-slip-type boundary conditions. However, in tropical cyclones, the boundary-layer module II is not much thinner than the bulk-vortex module I. The magnitude of the entrainment into the boundary layer constrains the secondary (radial/axial) flow in the bulk vortex. Under conservation of angular momentum in the inviscid bulk-vortex module for an axially invariant, potential vortex (generalized to the Earth-rotation-based non-inertial frame of reference), the absolute angular momentum is invariant both along and across streamlines. For such a vortex, the radial profile of the swirl at the top edge of the boundary layer is independent of the configuration of the secondary-flow streamlines in the bulk vortex. Detailed solution may be pursued first for the approximately incompressible dynamics in the boundary layer. But properties holding along the secondary-flow streamlines, and identified at the periphery of the bulk vortex, do constrain the radial profiles of thermodynamic fields holding at the top edge of the boundary layer under a generalized potential vortex. So, for purposes of quantifying the entrainment into the boundary layer, simple statements of a gradient-wind balance and conservation of angular momentum in the bulk vortex suffice to complete a lowest-order formulation of the dynamics in the boundary layer. Moreover, for purposes of quantifying the energetics in the boundary layer, it is possible to bypass quantifying the energetics within the bulk vortex. Key integrals for the energetics are invariant along (though not across) streamlines. By correlating influx to the bulk vortex (from the ambient) at the periphery, to efflux from the bulk vortex (to the boundary layer) at the top edge of the boundary layer, the radial profiles of thermodynamic fields holding at the top edge of the boundary layer are economically inferred. Incidentally, near the open-boundary periphery of a steady vortex, it is not evident that the swirl dominates the radial component of velocity.

Third, from figure 1, there is an interface between the unsaturated bulk-vortex fluid in I and the saturated ‘core’ fluid in III. The position of, and properties along, the interface remain to be found in the course of solution. The interface demarcates the boundary between two inviscid modules, so the position is set by the continuity of pressure (Carrier *et al.* 1971, pp. 149–150). The interface is: a streamline (more meticulously, a streamsurface, but that terminology is not adopted); a vortex sheet for the secondary (radial/axial) flow; and a contact surface. Any integral that is constant along streamlines is constant along the interface. In general, the constants differ across the indefinitely thin interface for integrals of the same physical quantity (i.e. same function or functional), because the streamlines of the inviscid module I transit the diffusive module II to enter the inviscid module III. Properties are transferred across streamlines in diffusive modules. However, fluid particles along those streamlines in close proximity to the interface have abbreviated residence in the boundary layer during transfer from the bulk vortex I to the lower core III. Accordingly, for reasons of

stability, the swirl, and thus the absolute angular momentum, are taken to be constant across the interface (Carrier *et al.* 1971, p. 149), although the swirl varies along the radially outwardly inclined interface (Palmèn & Newton 1969; Fendell 1974).

Fourth, a hurricane is more challenging to analyse than a tropical storm (or tropical depression) because a second such interface, between the unsaturated eye fluid in IV and the saturated core fluid in III, is present (figure 2). Again, the position of, and properties along, that interface remain to be found in the course of solution.

Fifth, just as there is a kilometre-thick frictional layer contiguous to the relatively immobile (on a volume-transport basis) ocean underlying the atmospheric vortex, so there could be a kilometre-thick frictional layer (not indicated in figures 1 and 2) contiguous to a relatively mobile tropopause overlying the vortex (Gill 1982, pp. 317–332). The swirl in the radial outflow, which becomes increasingly anticyclonic with increasing radial distance from the central axis (Palmèn & Newton 1969, p. 487–488), would be reduced to smaller-magnitude values across the thickness of the upper boundary layer. That is, the magnitude of the swirl would decrease as the upper boundary layer is traversed, at fixed radius, from lower edge to top edge. Moreover, fluid might be detraining from the upper boundary layer at most radii, just as fluid is being entrained into the bottom boundary layer at most radii. If so, then at the periphery, most of the throughput enters the vortex above the ocean-contiguous boundary layer, and exits the vortex below the tropopause-contiguous boundary layer, both influx and efflux being pressure-gradient-assisted.

A tractable approach for a steady-state, non-evolving model is to adopt, for given stratification at the peripheral boundary, tentative positions for the end points (more meticulously, end curves of circular shape) of the interface between modules I and III. For example, values of r'_{min} and $z'_{interface}$ may be varied, after z'_{edge} and r'_o are assigned. Solution of simultaneous nonlinear algebraic equations permits deduction of at least an approximation to the configuration of the entire interface between the modules. It may be anticipated that a solution consisting of physically plausible states within modules I and II exists for each of a range of choices of end points for the interface between modules I and III. In general, these solutions are of TD or TS intensity. For choices of end points implying sufficiently large spinup (because some fluid particles in the bulk vortex have closer approach to the axis of rotation under conservation of angular momentum), presumably no solution that is based on saturated ascent throughout the core exists. Condensational heat alone cannot generate a sea-level pressure anomaly sufficiently large to be consistent with intense spinup. However, via postulation of a suitably inserted, compressionally heated eye module, overlying a radially outwardly sloped eyewall (by choice of end points of the interface between modules III and IV), a sea-level pressure anomaly that is sufficiently large to be consistent with intense spinup is achievable. The trial-and-error investigation implicit in this outline suggests adoption of a simplistic, rapidly integrable formulation for each of the modules, to explore the range of possible configurations. For example, in a steady model, is eye insertion exactly coincident with achievement of a particular intensity (nominally, 33 m s^{-1}), or not?

3. The dynamics and energetics of the boundary-layer module

3.1. *Dynamics*

We first pursue solution for the boundary-layer flow over the large radial expanse from periphery to separation (wherever that occurs) because, as noted, the dynamics in the boundary-layer module constrains the secondary flow in the bulk vortex. The

steady axisymmetric flow is approximated as incompressible since the maximum speed achieved in a tropical cyclone rarely exceeds 100 m s^{-1}, so the Mach number rarely reaches even 0.3. The analysis is carried out in a non-inertial coordinate system rotating at the constant speed of that component of the rotation of the Earth which is normal to the local tangent plane. A simple down-gradient-diffusion model with a constant transfer coefficient, ascribed eddy-diffusion values, is examined, in the absence of observational evidence compelling the adoption of a more refined formulation. Other transfer models, however, are readily accommodated by the procedures developed below.

The conservation equations (Greenspan 1968, pp. 5–8) are

$$\nabla' \cdot \boldsymbol{q}' = 0, \tag{3.1}$$

$$\nabla'(q'^2/2) + (\nabla' \times \boldsymbol{q}') \times \boldsymbol{q}' + 2\boldsymbol{\Omega}_e' \times \boldsymbol{q}' = -\nabla'\tilde{p}' - \nu'\nabla' \times (\nabla' \times \boldsymbol{q}'), \tag{3.2}$$

where $\tilde{p}' = (p'/\rho_{ref}') - (\boldsymbol{\Omega}_e' \times \boldsymbol{r}')^2/2 + g'z'$, ρ_{ref}' denotes a reference density, the gravitational acceleration $\boldsymbol{g}' = -g'\hat{\boldsymbol{z}}$, the velocity in inertial coordinates $\boldsymbol{v}' = \boldsymbol{\Omega}_e' \times \boldsymbol{r}' + \boldsymbol{q}'$, the angular velocity of the earth is $\boldsymbol{\Omega}_E'$, the normal to the local tangent plane is $\hat{\boldsymbol{z}}$, $\boldsymbol{\Omega}_e' = \Omega'\hat{\boldsymbol{z}}$, $\Omega' = (\boldsymbol{\Omega}_E' \cdot \hat{\boldsymbol{z}})$, and ν' denotes the kinematic eddy viscosity.

Non-dimensionalization is introduced by letting

$$\boldsymbol{q} = \boldsymbol{q}'/(\Psi_o'\Omega')^{1/2}, \quad p = \tilde{p}'/(\Psi_o'\Omega'), \quad \boldsymbol{r} = \boldsymbol{r}'/(\Psi_o'/\Omega')^{1/2} \quad \text{and} \quad E = \nu'/\Psi_o', \tag{3.3}$$

where the Ekman number $E \ll 1$ for circumstances of interest, and Ψ_o' has the dimensions of a circulation. If Ψ_o' is ascribed the value of the maximum swirl speed times the radius at which the maximum occurs, non-dimensionalization would employ unknown outputs, rather than prescribed inputs. Thus, we follow Greenspan (1968, pp. 6–7) and set $\Psi_o' = \Omega' r_o'^2$ where r_o' denotes the radial extent of the cylindrical domain.

Thus,

$$\nabla \cdot \boldsymbol{q} = 0, \tag{3.4}$$

$$\nabla(q^2/2) + (\nabla \times \boldsymbol{q}) \times \boldsymbol{q} + 2\hat{\boldsymbol{z}} \times \boldsymbol{q} = -\nabla p - E\nabla \times (\nabla \times \boldsymbol{q}). \tag{3.5}$$

These non-dimensional equations are studied in axisymmetric cylindrical polar coordinates (it is convenient to reserve the symbol w)

$$\boldsymbol{q} = u\hat{\boldsymbol{r}} + v\hat{\boldsymbol{\theta}} + \tilde{w}\hat{\boldsymbol{z}}, \quad \boldsymbol{r} = r\hat{\boldsymbol{r}} + z\hat{\boldsymbol{z}}. \tag{3.6}$$

At the top edge of the boundary layer, the gradient-wind equation is adopted as a lowest-order approximation to the conservation of radial momentum:

$$\pi_r = 2V + V^2/r, \tag{3.7}$$

where, in the bulk vortex, $p(r, z) \to \pi(r)$, and $v(r, z) \to V(r)$, at the top edge of the boundary layer. For consistency with the boundary-layer solution, it is anticipated that the axial velocity component in the bulk vortex $\tilde{w}(r, z) \to E^{1/2}W(r)$ at the top edge of the boundary layer. This modest magnitude, in conjunction with continuity, suggests that, near the top edge of the boundary layer, the nonlinear convective terms in the radial-momentum equation are small relative to the terms retained in (3.7), at least at smaller radius where higher swirl holds.

If $\tilde{\zeta} = z/E^{1/2}$ (which implies that the boundary layer is $O(E^{1/2})$ in thickness relative to r_o'), and if in the boundary layer

$$\left.\begin{aligned} u = u_b(r, \tilde{\zeta}) + \cdots, \quad v = v_b(r, \tilde{\zeta}) + \cdots, \quad \tilde{w} = E^{1/2}w_b(r, \tilde{\zeta}) + \cdots, \\ p = p_b(r, \tilde{\zeta}) + \cdots, \end{aligned}\right\} \tag{3.8}$$

then the axial component of the momentum-conservation equation (3.5) takes the conventional form $(\partial p_b/\partial\tilde{\zeta}) = 0$, and the pressure field in the boundary layer is found from (3.7) if $V(r)$ is known. If

$$\psi = rv_b, \quad \Psi = rV, \quad \phi = ru_b, \quad w = 2^{-1/2}w_b, \quad x = r^2, \quad \zeta = 2^{1/2}\tilde{\zeta}, \tag{3.9}$$

then, in terms of dimensional quantities,

$$\left.\begin{aligned} \phi = r'u'/(\Omega' r_o'^2), \quad \psi = r'v'/(\Omega' r_o'^2), \quad w = w'/(2\Omega' v')^{1/2}, \\ \zeta = z'/(v'/2\Omega')^{1/2}, \quad x = r'^2/r_o'^2, \end{aligned}\right\} \tag{3.10}$$

the boundary-layer thickness being $O(v'/\Omega')^{1/2}$. Introduction of (3.8) and (3.9) into (3.4) and (3.5) gives

$$\phi_x + w_\zeta = 0, \tag{3.11}$$

$$\phi\phi_x + w\phi_\zeta + (\Psi^2 - \psi^2 - \phi^2)/2x - (\psi - \Psi) - \phi_{\zeta\zeta} = 0, \tag{3.12}$$

$$\phi\psi_x + w\psi_\zeta + \phi - \psi_{\zeta\zeta} = 0. \tag{3.13}$$

Patching to the bulk vortex gives, with $\Psi(x)$ taken as known and ζ_{edge} anticipated to be 'large',

$$\zeta \to \zeta_{edge} : \phi \to 0; \quad \psi \to \Psi(x). \tag{3.14}$$

On $\zeta = 0$, no-slip conditions at a boundary impervious to convection are adopted:

$$\zeta = 0 : \phi = \psi = w = 0. \tag{3.15}$$

For the modest flow speeds holding in the vicinity of the periphery at $x = 1$, the nonlinear terms in (3.11)–(3.13) may be discarded as negligible relative to the linear terms. The solution to the linear balance of Coriolis 'force', pressure force, and friction, in which x enters parametrically only, was given by Ekman:

$$\phi \approx -[\Psi(x)]\sin(2^{-1/2}\zeta)\exp(-2^{-1/2}\zeta), \tag{3.16}$$

$$\psi \approx [\Psi(x)][1 - \cos(2^{-1/2}\zeta)\exp(-2^{-1/2}\zeta)], \tag{3.17}$$

$$w \approx 2^{-1/2}[\Psi_x(x)]\{1 - [\sin(2^{-1/2}\zeta) + \cos(2^{-1/2}\zeta)][\exp(-2^{-1/2}\zeta)]\}. \tag{3.18}$$

Of particular interest is the boundary-layer exchange with the overlying vortex, $w(x, \zeta \to \zeta_{edge}) \equiv W(r)$ for $\Psi(x)$ of interest. For $x \to 1$, from (3.18)

$$w(x \to 1, \zeta \to \zeta_{edge}) \equiv W(x) \to 2^{-1/2}\Psi_x(x). \tag{3.19}$$

It is possible (according to Carrier 1971*a*) that (3.19) approximates adequately the exchange even for values of x sufficiently smaller than unity that (3.16)–(3.18) do not approximate adequately the solution to (3.11)–(3.15). We shall check this suggestion. In any case, dependence on the parameter v' is displayed mainly in (3.10), since v' does not appear in the boundary-value problem for $\phi, \psi, w, \Psi, \zeta$ and x, except implicitly in the quantity ζ_{edge}.

Since the absolute angular momentum is taken to be invariant along and across streamlines in module I, according to prior discussion, then, dimensionally, in the bulk vortex

$$r'v'(r') + \Omega' r'^2 = r_o' v_o' + \Omega' r_o'^2, \tag{3.20}$$

where $v'(r_o')$, denoted v_o', is regarded as known. Hence, under the non-dimensionalization discussed in (3.3) and thereafter, and in (3.9),

$$\Psi(r) = rV(r) = 1 + \varepsilon - x, \quad \varepsilon \equiv v_o'/(\Omega' r_o'), \tag{3.21}$$

where $0 < \varepsilon \ll 1$ for parameter values of practical interest. Thus, ε, which may be characterized as a Rossby number (Greenspan 1968, p. 7), is significant near $x = 1$ only, and is not used to scale variables. The circulation in module I above the boundary layer is stable (Greenspan 1968, pp. 271–272). There is downflow into the boundary layer as $x \to 1$ (and wherever (3.19) suffices). For values of $(2\Omega' \nu')^{1/2}$ of physical interest, the downflow is a very modest downdrift, according to (3.10).

However, accumulatively over x, the downdrift implicit in (3.19) and (3.21) implies a significant radial inflow ϕ within the boundary layer. Very little of this radial inflow stems from influx over ζ at $x = 1$, from (3.16) and (3.21) for $\varepsilon \to 0$. Moreover, as x decreases, the peak value Ψ of relative angular momentum ψ increases appreciably, from (3.14) and (3.21). Thus, on the left-hand sides of both (3.12) and (3.13), the nonlinear acceleration terms dominate the Coriolis term as x decreases. However, whereas, in the conservation of angular momentum equation (3.13), friction balances nonlinear advection across the entire boundary layer as x decreases, the presence of x in the denominator of some nonlinear terms suggests that an analytically convenient, purely inviscid balance approximates the conservation of radial momentum equation (3.12) over the majority of the thickness of the boundary layer as x decreases (Burggraf, Stewartson & Belcher 1971; Carrier 1971*a*; Belcher, Burggraf & Stewartson 1972; Carrier *et al.* 1994):

$$\phi^2 + \psi^2 \approx \Psi^2. \tag{3.22}$$

Thus, at any fixed small value of x at which (3.21) holds, ψ monotonically decreases to zero, from a peak value near $(1 + \varepsilon)$, as ζ decreases, whereas ϕ monotonically increases from zero to a peak value approaching $(1 + \varepsilon)$. However, for small x, a two-layer substructure must develop because, in the immediate proximity of the sea surface $\zeta = 0$, the inflow ϕ must rapidly decrease from its peak value to zero within a relatively thin, swirl-free, frictional sublayer, to comply with the no-slip constraint (3.15). The evolution of the boundary-layer structure, from Ekman-layer profiles to a substantially different, two-layer, partially inviscid character, has noteworthy implications for the boundary layer (and, as it turns out, for other modules of the tropical cyclone). Selecting a uniformly suitable set of basis functions for a method-of-weighted-residuals integration is challenging in view of this change of behaviour with x. Wherever (3.22) holds to good approximation, turbulent diffusion plays a diminished role, and the details of the eddy-diffusion coefficient are of reduced importance. The plausibility argument just given for (3.22) is supported by more quantitative argument (Carrier *et al.* 1994, Appendix B.2).

Numerical integration of the one-parameter parabolic boundary-value problem (3.11)–(3.18) under (3.21) is pursued to elucidate, *inter alia*: the intermediate behaviour during transition with x from Ekman-layer to two-layer structure; how well (3.22) is approximated at 'small' x (to be characterized); and the magnitude of departure at 'small' x of $W(x)$ from the Ekman value, $-2^{-1/2}$. The integration may be continued to smaller x as long as (3.21) continues to hold, i.e. until the boundary layer separates and the formulation fails at some finite x. Clearly, separation is anticipated to arise at larger x for a less intense vortex. That a 'global' solution may be completed by finding plausible results for companion modules remains to be demonstrated.

The numerical integration may be pursued with conventional method-of-lines software, but typically only after transformation to von Mises coordinates (Belcher *et al.* 1972) to remove explicit presence of $w(x, \zeta)$ in (3.12) and (3.13). Thus, for the convenience of retaining (x, ζ) coordinates, a code with a highly stable variant of Crank–Nicolson-type differencing (e.g. Pearson 1986) was written. First-order finite-

differencing with steps of 0.005 in the time-like coordinate x generates, at each x, a two-point boundary-value problem in the space-like coordinate ζ for ϕ and ψ, solved with fourth-order differencing with steps of 0.02 over $0 \leqslant \zeta \leqslant 9$. The function $w(x, \zeta)$ is then computed from (3.11). A typical case is run in roughly two minutes on a standard laptop, a property which is noteworthy regarding real-time operational use.

As confirmed later, the value $\zeta = \zeta_{edge} = 5$ approximates well the thickness of a boundary layer that is effectively frictionless as its top edge. Taking $\zeta_{edge} = 5 = z'_{edge}/(\nu'/2\Omega')^{1/2}$ from (3.10), for the observed value $z'_{edge} = 1$ km, with $\Omega' = 1.74 \times 10^{-5}$ s^{-1} at about 14° latitude, we find $\nu' \approx 1.4$ m^2 s^{-1}, Pedlosky (1987, pp. 184–185) discusses uncertainties in the assignment of value to the eddy viscosity for vertical transport near the Earth's surface. Since (3.10) gives the physical thickness of the boundary layer to be proportional to $\nu'^{1/2}$, and since current estimates (§ 2.3) give the plausible range of the tropical-cyclone-boundary-layer thickness to be 0.5–2 km, the consistent range of values of the eddy viscosity is limited to one-quarter to four times the value assigned above. Thus, the largest value for ν' plausibly admitted by our model is but 16 times the smallest value. Explicitly, $\nu' \approx 0.01$ m^2 s^{-1} results in a boundary-layer thickness of 100 m, and $\nu' \approx 0.1$ m^2 s^{-1} results in thickness of about 300 m, both unlikely values; $\nu' \approx 0.5$ m^2 s^{-1} results in about 700 m, a more plausible value. Thus, the admissible range for ν' is tightly constrained, and the sensitivity of the solution over this range relates to layer thickness. Also from (3.10), the vertical velocity component w' (and thus the total throughput in mass/time) is proportional to $\nu'^{1/2}$. The time-averaged entrainment rate into the boundary layer, $|w'_{edge}|$, is $O(0.7$ cm s$^{-1})$, for the nominal value of ν', a speed much too small to be readily detected, as previously noted (Carrier *et al.* 1971). Increasing or decreasing this very modest mean downdrift by a factor of two would have negligible consequence for the challenge of its detectability.

An alternative option for empirically assigning value to the eddy viscosity might entail matching output from the time-averaged model to observed near-sea-surface velocity profiles from individual, slowly descending, long-resident-time dropsondes. However, measured near-ocean-surface velocity profiles for the important, high-speed portion of the vortex are extremely rare, and those available do not correspond with any boundary-layer logarithmic-profile law (Black *et al.* 2012; see also Smith & Montgomery 2012). Perhaps this behaviour should not be unexpected because the observed aerodynamic roughness of the ocean surface is highly dependent on the wind speed, the roughness increasing appreciably with wind speed up to about 40 m s^{-1}, then decreasing to virtually zero by speed of about 80 m s^{-1}, so the surface becomes extremely smooth in the most intense part of major hurricanes (wind speed $>$50 m s^{-1}) (Holthuijsen, Powell & Pietrzak 2012). Thus, this alternative does not seem viable for 'calibrating' a simplistic model.

Figure 3 presents the downdraft $W(x; \varepsilon)$ as a function of x for a given value of ε, with effective invariance found to hold for $\varepsilon \leqslant 10^{-3}$. The downdraft is seen to remain at roughly twice the Ekman value over $1 \geqslant x \geqslant 0.25$ or $1 \geqslant r \geqslant 0.5$, or for at least 75 % of the interfacial area between modules I and II. For smaller x, the downdraft increases relatively rapidly, achieving, at $x \approx 0.05$, five times the Ekman value. Carrier's suggestion (Carrier 1971*b*, figure 8) that the Ekman value suffices to characterize the magnitude of the downdrift at all x until separation is better than might appear at first because what is of primary interest is the normalized mass per time entering the boundary layer. The *radially integrated* normalized mass per time entering the boundary layer, $\eta(x, \zeta_{edge})\{\equiv [\eta'(r', z'_{edge})]/[\rho'_{ref}\Omega' r'^3_o (E/2)^{1/2}]\}$,

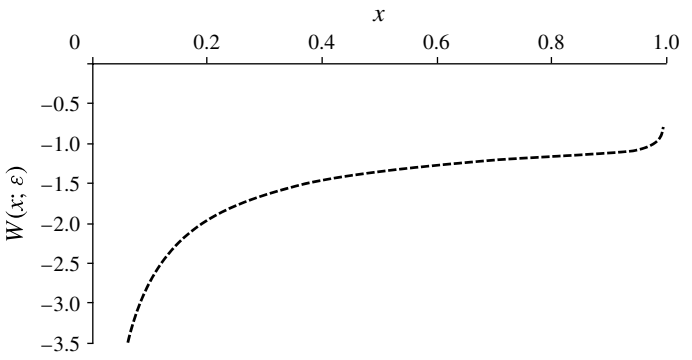

FIGURE 3. The dimensionless downdraft at the top edge of the boundary layer, $W(x;\varepsilon)$, as a function of the square of the radial distance from the axis, x, which is normalized so the periphery is $x = 1$. The results are effectively invariant of the parameter ε for $\varepsilon \leqslant 10^{-3}$. A physically small downdraft persists until separation for the swirl profile (3.21), and, in fact, monotonically increases in magnitude with decreasing x.

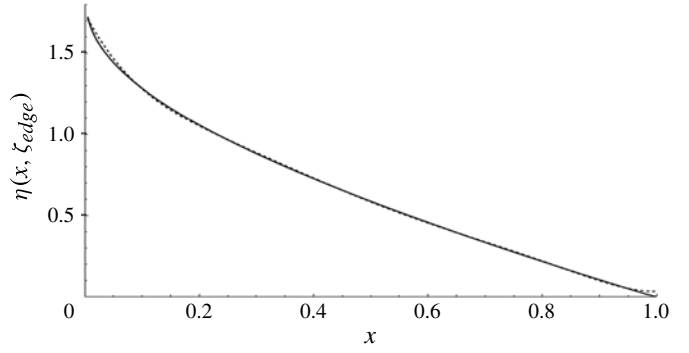

FIGURE 4. The dimensionless accumulative downdraft at the top edge of the boundary layer, $\eta(x, \zeta_{edge})$, normalized against $\rho'_{ref}\Omega' r_0'^3 (E/2)^{1/2}$, versus x, for $\varepsilon \leqslant 10^{-3}$, from numerical integration (solid curve). This is the downflux integrated over x, starting from the effectively null value at the periphery $x = 1$, and continuing to smaller x until separation. Also depicted is a convenient polynomial curve fit (dashed curve) $32.31x^6 - 105.32x^5 + 135.2x^4 - 87.10x^3 + 30.12x^2 - 6.948x + 1.749$.

is $\int_1^x W(y;\epsilon)\,\mathrm{d}y$. The integral is plotted in figure 4, along with a polynomial curve fit. The integral $\eta(x, \zeta_{edge})$, also denoted $\eta_{edge}(x)$, is just the streamfunction evaluated at the boundary-layer top edge. This statement is clarified with the aid of (3.23), below.

Figures 5–7 presents profiles versus ζ of $\phi(x, \zeta)$, $\psi(x, \zeta)$, and $w(x, \zeta)$, respectively, at each of several values of x. In addition, figure 8 presents isopleths of $\phi(x, \zeta)$. Figures 5 and 8 reflect the large evolution of the inflow ϕ, from a modest-magnitude oscillatory profile at $x \approx 1$ to a one-signed profile with an ever-increasing peak magnitude as $x \to 0$. From figure 7, the downdraft w supports this peak. In contrast, from figure 6, the profiles of relative angular momentum ψ evolve little in shape, as $x \to 0$, other than to reflect the larger value holding at $\zeta = \zeta_{edge}$. The small-x results presented in figures 5 and 6 are remarkably consistent with boundary-layer

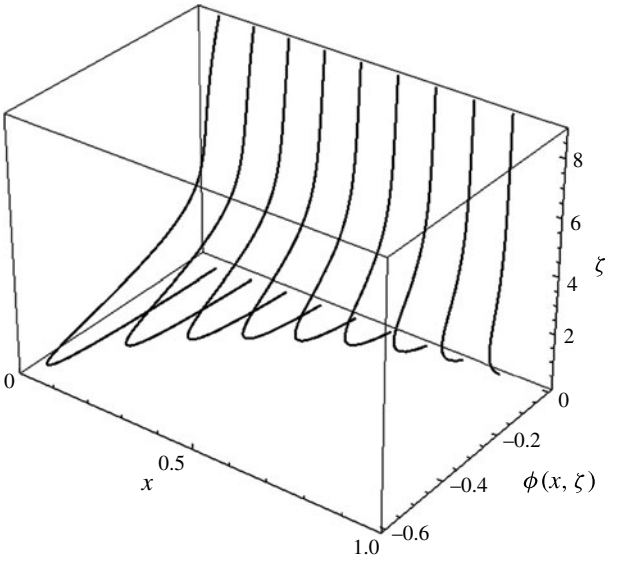

FIGURE 5. For the potential vortex (3.21) with $\varepsilon = 10^{-3}$, the normalized radially inward flow in the boundary layer, $\phi(x, \zeta)$, versus the transverse coordinate ζ, at nine uniformly spaced values of the streamwise coordinate x spanning the range $(0.07, 0.87)$. Definitions are given in (3.10). The peak inward flow increases significantly in magnitude relative to $\Psi(x; \varepsilon)$ as x decreases, and occurs at smaller ζ.

measurements via laser-Doppler anemometers for the potential-vortex portion of a laboratory Rankine vortex (Phillips & Khoo 1987).

An indication of the approach of the solution to a two-layer substructure is afforded by (figure 9) contours of the sum $[\phi^2(x, \zeta) + \psi^2(x, \zeta)]^{1/2}$ versus ζ at several small values of x. According to the estimate (3.22), this sum would be constant over ζ at the constant value $\Psi(x)$. Indeed, the computed sum is constant over ζ, except for $\zeta \to 0$, for sufficiently small x. Another indication is provided by the contrasting profiles of the frictional term $\phi_{\zeta\zeta}(x, \zeta)$ versus ζ at several values of x (figure 10), and of $\psi_{\zeta\zeta}(x, \zeta)$ versus ζ at the same values of x (figure 11). At small x, friction contributes to the conservation of radial momentum only near $\zeta = 0$ (figure 10), but, in contrast, continues to contribute to $\zeta \approx 5$, though not beyond, in the conservation of angular momentum (figure 11). The integration is pursued to $\zeta = 9$ to confirm these statements.

Contours (figure 12) of the streamfunction $\eta(x, \zeta)$, defined by

$$\partial\eta(x, \zeta)/\partial x = w(x, \zeta) \quad \text{or} \quad \partial\eta(x, \zeta)/\partial\zeta = -\phi(x, \zeta), \tag{3.23}$$

with $\eta(x, 0) = 0$ by (3.14), $\eta(1, \zeta) \approx 0$ by (3.15) and (3.21), indicate that fluid particles entering the boundary layer at larger x, for which $\Psi(x)$ is smaller, may flow closer to the sea surface, and may experience significant frictional forces longer. These particles may penetrate closer to the axis than fluid particles that enter the boundary layer at smaller x. But the latter particles enter with larger $\Psi(x)$, and are subject to friction over a smaller span in x if they emerge from the boundary layer further from the axis than particles that enter at larger x. The upshot is that expectations of significant spinup within the boundary layer exceeding the peak swirl achieved in the bulk vortex

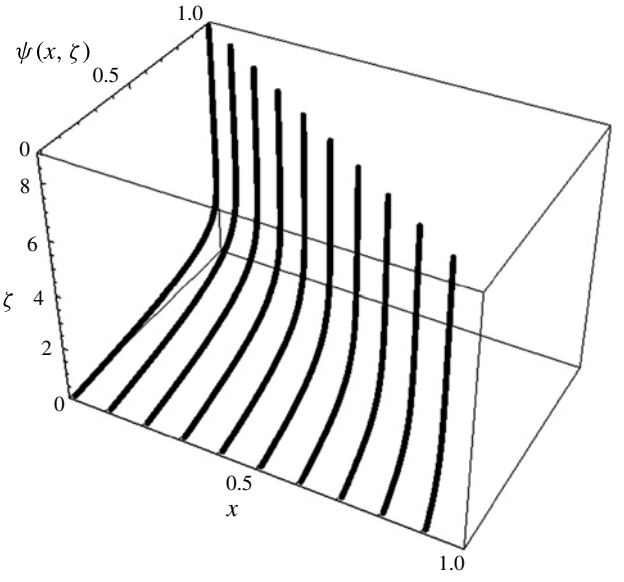

FIGURE 6. For the case presented in figure 5, profiles of the normalized relative angular momentum, $\psi(x, \zeta)$, defined in (3.10), at ten uniformly spaced values of x spanning the range (0.005, 0.905). In general, each profile approaches its asymptotic value at $\zeta \approx 5$, although the calculation is over the range $0 \leqslant \zeta \leqslant 9$. The monotonic profiles increase to a larger asymptotic value as x decreases, but change little in shape.

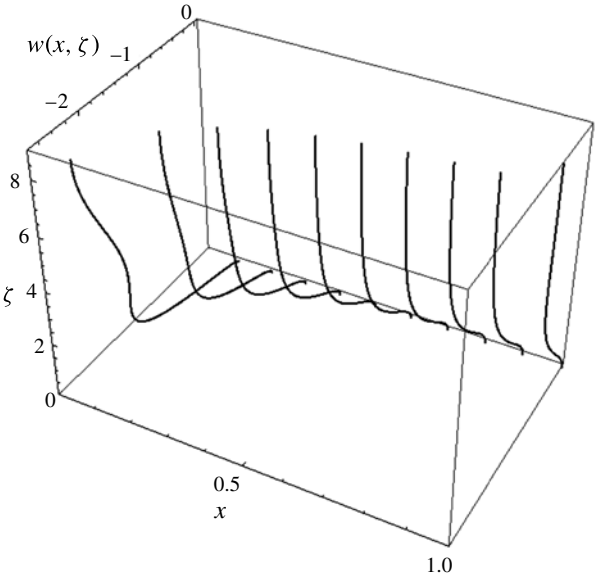

FIGURE 7. For the case presented in figure 5, profiles of the normalized axial velocity component, $w(x, \zeta)$, defined in (3.10), at ten uniformly spaced values spanning the range (0.1, 1.0). A downflux holds over all finite ζ at any x, the downflux monotonically increasing in magnitude as x decreases. Thus, fluid in the boundary layer uniformly drifts seaward as the fluid moves toward the axis, to support a continually increasing near-sea-surface radial influx.

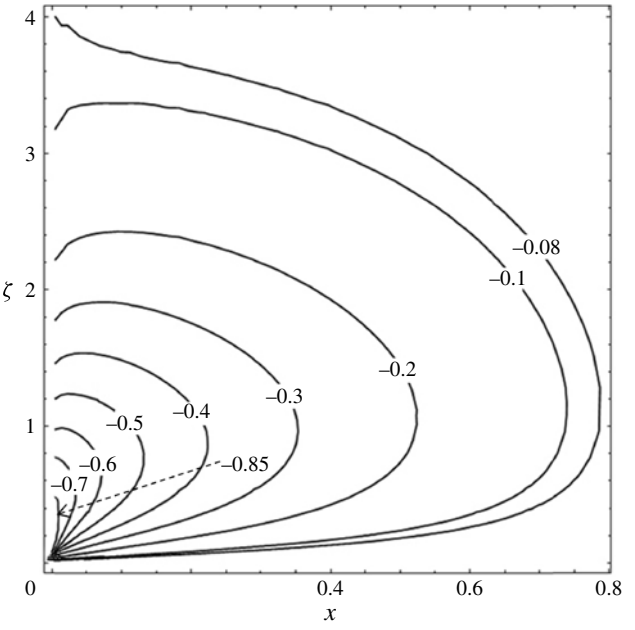

FIGURE 8. For the case presented in figure 5, some isopleths of the normalized radially inward flow $\phi(x, \zeta)$. For a boundary layer persisting to: $x = 0.1$, $\phi_{peak}/\Psi \approx 5/9$; and to $x = 0.005$, $\phi_{peak}/\Psi \approx 0.95$ (not shown). Since $x = (r'/r'_o)^2$, for $r'_o = 300$ km, $x = 0.005$ corresponds to ∼20 km.

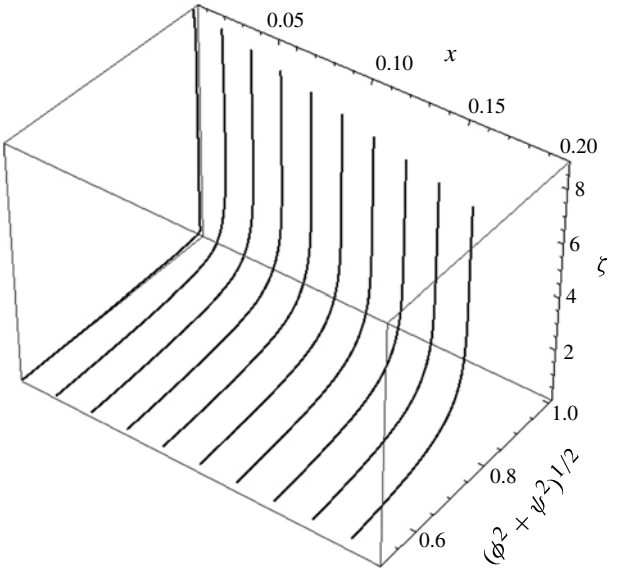

FIGURE 9. For the case presented in figure 5, the profile of $[\phi^2(x, \zeta) + \psi^2(x, \zeta)]^{1/2}$ versus ζ at each of ten uniformly spaced values of x spanning the range $(0.005, 0.185)$. From the discussion of (3.22), approximate constancy of the square-root expression at the value $\Psi(x)$ indicates, for each x, the values of ζ for which the conservation of radial momentum in the boundary layer (3.12) is effectively non-diffusive, under the high-swirl, near-axis portion of the vortex.

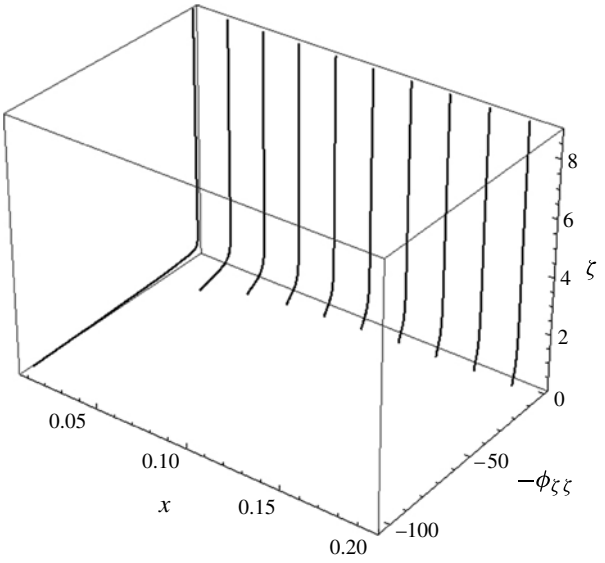

FIGURE 10. For the case presented in figure 5, the frictional term $-\phi_{\zeta\zeta}(x, \zeta)$ in (3.12), the conservation of radial momentum in the boundary layer, plotted at each of ten values of x spanning the range $(0.005, 0.185)$. The magnitude of the frictional term is virtually nil above an ever-thinning sublayer contiguous to $\zeta = 0$, as x decreases. This behaviour is consistent with the results displayed in figures 5, 8, and 9.

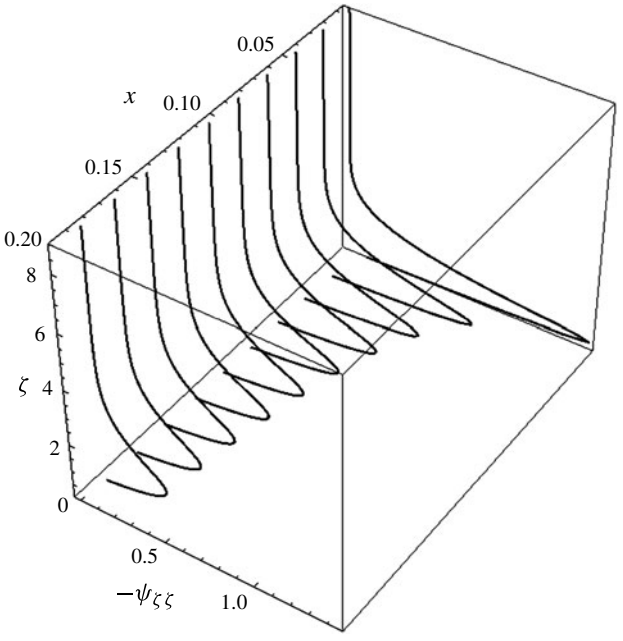

FIGURE 11. For the case presented in figure 5, the frictional term $-\psi_{\zeta\zeta}(x, \zeta)$ in (3.13), the conservation of angular momentum in the boundary layer, plotted at each of ten values of x spanning the range $(0.005, 0.185)$. The magnitude of the frictional term typically increases at any ζ as x decreases, in contrast to the behaviour of $-\phi_{\zeta\zeta}(x, \zeta)$ displayed in figure 10.

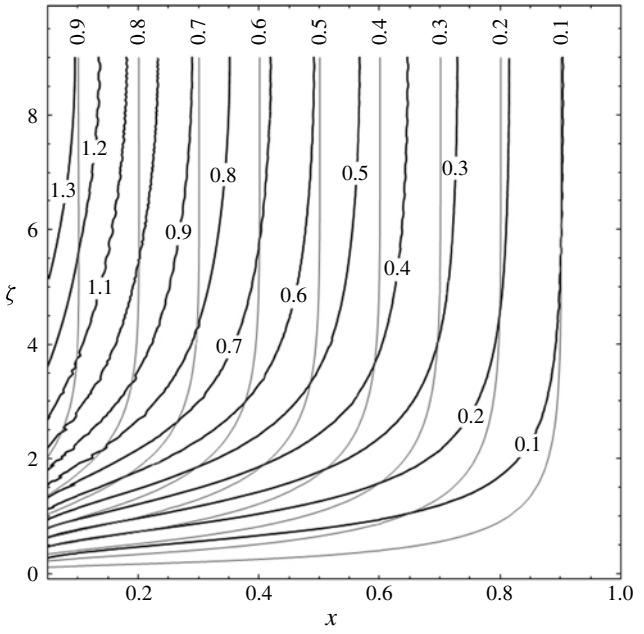

FIGURE 12. For the case presented in figure 5, normalized streamlines (darker contours, with horizontal labels) in the boundary layer as given by (3.23) and associated boundary condition, for streamlines entering the frictional layer at large ζ for x in the range (0.1, 1). Superimposed are isopleths (lighter contours, with vertical labels) of the relative angular momentum $\psi(x, \zeta)$. The fluid particles likely to penetrate closest to the axis have relatively modest values of $\psi(x, \zeta)$, so noteworthy 'overshoot' of (say) $\Psi(0.01)$, prior to detrainment from the boundary layer, appears questionable.

(such an excess being sometimes referred to as 'swirl overshoot') may be exaggerated (Carrier *et al.* 1994, Appendix D).

Laboratory evidence of the two-layer substructure at smaller x is reported for the turbulent boundary layer under a potential vortex (Burggraf *et al.* (1971) pp. 1832–1833; see also Phillips & Khoo 1987). A few isolated instantaneous measurements of boundary-layer velocity profiles in tropical cyclones have been obtained by dropwindsondes, but no sustained sampling to provide a statistical distribution for comparison with the mean distribution sought by this modelling.

3.2. *Energetics*

Close examination of energetics-related properties of the tropical-cyclone boundary layer, when averaged over a time scale longer than any local convective process, has been often bypassed in the literature. In the context of accounting for boundary-layer effects on the entire vortex, generally focus has been on applying bulk-aerodynamic relations to quantify the transfer of sensible and latent heat at the sea–air interface. Such relations are formal, dimensionless statements of little utility until the embedded transfer coefficients are appropriately assigned; until then, the relations merely express one unknown in terms of another. While research continues, the often adopted and speculative extrapolation to high-wind-speed conditions of the wind-speed dependence holding for the transfer coefficients at relatively modest wind speed (e.g. Riehl 1979) has been shown to be observationally invalid (Bell, Montgomery & Emanuel 2012),

and to result in erroneous overestimates of sea–air transfer of enthalpy at high wind speed (Haus *et al.* 2010; Zhang *et al.* 2011; Holthuijsen *et al.* 2012). It is disconcerting that intensity-related results obtained from many, if not most, tropical-cyclone models are very sensitive to the uncertain values assigned to parameters appearing in conventional formulations of boundary conditions at the air–sea interface (Eliassen & Lystad 1977; Montgomery, Smith & Nguyen 2010). Here, care is taken to incorporate the enthalpy transport into the boundary layer associated with downdrift from the overlying bulk-vortex module (Carrier *et al.* 1971; Fendell 1974), as an important complement to roughly ambient-level sea–air transfer of enthalpy.

The point of view expressed in the last paragraph (that the majority of the heat-and-moisture content of the throughput being processed in the core of the vortex is already in the atmosphere of the autumnal maritime tropics, and greatly enhanced sea-to-air transfer of enthalpy under the high-speed portion of the vortex to enrich the throughput is neither necessary nor plausible) is distinctly a minority one, which traces back to Carrier *et al.* (1971, pp. 159–170). An alternative, far more commonly adopted point of view is that proposed by Emanuel (2005, pp. 56–57; see also the references cited therein):

> '... air flowing from high to low pressure would cool were no heat added to it... [H]eat flowing from sea into the air keeps it at nearly constant temperature. But there is a much more important source of heat: the enormous flow of energy that occurs when sea water evaporates into the inflowing air... [E]vaporation... effective in driving the storm occurs very near the hurricane's eyewall, where the winds are strongest. When hurricanes make landfall, they quickly die because they are cut off from their oceanic energy source.'

In fact, isentropic thermodynamic relations are not pertinent to, and thus an inappropriate basis for anticipations about, properties of flow in frictional boundary layers; nearly saturated sea-level air can accept but little additional moisture; and hurricanes would die in two hours after landfall on even non-orographic coastlines were moment-to-moment enthalpy transfer crucial to their moment-to-moment maintenance, but hurricanes decay on (an inertial) time scale of 8–12 h after landfall.

Nevertheless, distractive controversies about sea-to-air enthalpy transfer persist because tropical cyclones involve an extreme environment, and the conditions are difficult to reproduce for corroboration of measurements. *In situ* observations of the core of the vortex remain particularly sparse, and those few readings available, even if possibly atypical, are meticulously examined. Enhanced sea-to-air transfer of enthalpy under the eye of a tropical cyclone has been cited as the plausible source of high-entropy air reported near the sea surface in a *small* number of hurricanes (Persing & Montgomery 2003; Montgomery *et al.* 2006; Bell & Montgomery 2008). In any case, simple consideration of the relative lateral dimensions in a hurricane of the bulk vortex and of the base of the eye readily supports the findings of numerical models, namely, the practical significance for vortex intensity of any such local enhancement of sea-to-air transfer under the eye is nil (Bryan & Rotunno 2009, and references cited therein).

For an incompressible model of the steady axisymmetric boundary-layer dynamics, the energetics is decoupled from the dynamics. Under the Reynolds analogy (so the turbulent Prandtl and Schmidt numbers are unity) (Eckert & Drake 1962) and the hydrostatic approximation, Carrier *et al.* (1971) adopt the relation

$$u'(\partial E'/\partial r') + w'(\partial E'/\partial z') = \nu'(\partial^2 E'/\partial z'^2), \tag{3.24}$$

where, for a perfect gas with constant heat capacity c_p' over the range of temperatures of interest, the total stagnation energy E' is given by

$$E' \equiv c_p' T' + L' Y' + g' z' + q'^2/2. \tag{3.25}$$

Here, T' denotes temperature; L' the relevant latent heat of phase transition for water substance; and Y' the mass fraction (or, to the accuracy being pursued here, alternatively regarded as the mixing ratio) of water vapour. To be sure, Y' is inherently dimensionless, but we make this one exception in notation because we wish to emphasize the dependence on dimensional arguments. In (3.24), we have followed Carrier *et al.* (1971) in neglecting dissipation as a minor contributor to the total energy balance in a low-Mach-number, high-Reynolds-number flow. We depart from Carrier *et al.* (1971) in also ignoring radiative transfer because our steady model is being applied to a lower-atmospheric phenomenon of tropical-cyclone scale and of duration on the order of a week (Houghton 1986, p. 15). For the boundary layer, observationally unsaturated virtually everywhere on a long-time average,

$$u'(\partial Y'/\partial r') + w'(\partial Y'/\partial z') = \nu'(\partial^2 Y'/\partial z'^2). \tag{3.26}$$

Although the boundary-layer-scaled coordinates have yet to be introduced, we have anticipated that the transversely diffusive terms dominate in (3.24) and (3.26) (Zhang *et al.* 2011). The convective coefficients $u'(r', z')$ and $w'(r', z')$ are available from the previously treated dynamics, so the transport equations (3.24) and (3.26) are linear parabolic convective–diffusive balances. Carrier *et al.* (1971, p. 160) characterize this formulation of the energetics as one in which '…the water vapour plays a important role in heat transfer *only* as a source of latent heat'.

For even a 100 m s^{-1} vortex, the contribution of the kinetic energy term $q'^2/2$ to the sum E' is uniformly $\leqslant O(1\,\%)$, and for many (though not all) purposes, $E' \to H' \equiv c_p' T' + L' Y' + g' z'$. Within the boundary layer, even a relatively thick boundary layer, the gravitational term is a small contributor to E', $\leqslant O(3\,\%)$.

The boundary conditions are now addressed. At the *nominal* sea surface $z' = 0$, the temperature is taken constant at all radii at the known ambient level $T'_{amb,s}$, any change (probably a noteworthy decrement, especially under the core for slower-translating vortices) being neglected, in accord with prior remarks (§ 2.2). At the sea surface, the relative humidity $RH'(r', 0)$ also is taken to be constant, at all radii, at the known ambient level $RH_{amb,s}$, the value being fairly close to (but less than) unity. Since $z' = 0$ has been taken to be the datum for the gravitational potential (see below (3.2)), and in view of the no-slip approximation (3.15):

$$E'(r', 0) = c_p' T'_{amb,s} + L' Y'(r', 0), \quad E'_{amb,s} \equiv c_p' T'_{amb,s} + L' Y_{amb,s}, \tag{3.27}$$

where, if $P'(T')$ denotes the saturation vapour pressure for water substance, exponentially dependent on temperature T',

$$Y'(r', 0) = \sigma RH_{amb,s} P'(T'_{amb,s})/p'(r', 0), \quad Y_{amb,s} \equiv \sigma RH_{amb,s} P'(T'_{amb,s})/p'_{amb,s}, \tag{3.28}$$

and σ denotes the ratio of the molecular weight of water vapour to that of dry air, ≈ 0.622.

At the periphery of the domain $r' = r'_o$

$$E'(r'_o, z') \approx H'(r'_o, z') = c_p' T'_{amb}(z') + L' Y'_{amb}(z') + g' z', \tag{3.29}$$

$$Y'(r'_o, z') = Y'_{amb}(z'), \tag{3.30}$$

Pressure (hPa)	T' (°C)	RH (%)	Mixing ratio (g/kg)	θ'_e (K)
500	−6.9	45	2.10	332
700	8.6	57	5.83	329
850	17.3	74	11.12	334
1000	26.0	81	17.92	345
1015.1	26.3	84	18.54	345

TABLE 1. Sampling from the Jordan mean ambient for the autumnal maritime tropics (Dunion & Marron 2008, p. 5250). (Notes. The equivalent potential temperature θ'_e is closely related to the total static energy $H'(r'_o, z')$ defined in (3.29). Jordan (1958) provides data on a finer grid.)

where $T'_{amb}(0) = T'_{amb,s}$ and $Y'_{amb}(0) = Y_{amb,s}$. More specifically, $T'_{amb}(z')$ and $RH'_{amb}(z')$ are here typified by the Jordan mean sounding for the maritime autumnal tropical ambient in the western Atlantic (see table 1) (Jordan 1958; Dunion & Marron 2008). Although this observational ambient profile extends from nominal sea level to 500 hPa only, this suffices for current (though not all) purposes. Dunion & Marron emphasize that the distribution of individual soundings for which table 1 provides the mean data is bimodal, virtually all the individual soundings being convectively unstable but more moist or drier than the mean, and the mean itself being infrequently observed. We have followed Carrier *et al.* (1971) and many others in focusing on the Jordan mean sounding, but we note that the mean, while convenient, might not have special relevance for the stratification holding at the periphery of a tropical cyclone.

The following standard approximate relations seem adequate for our purposes for relating thermodynamic variables:

$$p'_a = \rho'_a R'_a T', \quad \sigma p'_{vap} = \rho'_{vap} R'_a T', \quad Y' = \rho'_{vap}/\rho' \approx \rho'_{vap}/\rho'_a, \quad \gamma = c'_p/(c'_p - R'_a), \tag{3.31}$$

$$RH' = p'_{vap}/P'(T'), \quad p' = p'_a + p'_{vap}, \quad \rho' = \rho'_a + \rho'_{vap}, \tag{3.32}$$

$$p' - (1-\sigma)p'_{vap} = \rho' R'_a T', \tag{3.33}$$

where subscript a denotes dry air, subscript vap denotes water vapour, R'_a denotes the gas constant for dry air, and γ denotes the ratio of specific heats for the mixture. The relations are inserted here because they enter into converting ambient sounding data from pressure coordinate p' (as in table 1) to the axial spatial coordinate z', e.g., for purposes of (3.29) and (3.30). In this connection, the hydrostatic relation suffices at the periphery $r' = r'_o$:

$$\partial p'/\partial z' = -\rho' g'. \tag{3.34}$$

We now address the inconsistency with (3.23), and with the boundary-layer dynamics in general, for which perforce an incompressibility approximation was adopted. The small-magnitude oscillatory inflow/outflow described by (3.16) at $x = 1$ suggests that the small amount of influx across the periphery directly into the boundary layer is of modest consequence for the boundary-layer energetics. The relations (3.29)–(3.34) are pertinent also to the aggregationally important inflow across the periphery into the bulk vortex, to be discussed in § 4; this inflow, at altitudes above the boundary layer, eventually enters the boundary layer. The incompressible approximation for the

boundary-layer dynamics has a bearing on the radial distribution during entrainment of the energetics-related fields, as next discussed.

The formulations in (3.24), (3.27), and (3.29) for $E'(r', z')$ in the boundary layer, and in (3.26), (3.28), and (3.30) for $Y'(r', z')$, are complete, upon specification at the top edge of the boundary layer of the profiles $E'(r', z'_{edge})$ and $Y'(r', z'_{edge})$. As implied in the introduction, and developed in detail in § 4 on the inviscid, steady flow in the bulk vortex I, values of four functions/functionals are invariant along streamlines in I, although the values vary from streamline to streamline (except for the absolute angular momentum, which is taken to be invariant from streamline to streamline). The four integrals include $Y'(r', z')$, and $E'(r', z')$, so $Y'(r', z') = Y'[\eta'(r', z')]$ and $E'(r', z') = E'[\eta'(r', z')]$, with $Y'[\eta'(r', z')]$ and $E'[\eta'(r', z')]$ inferred from the Jordan mean sounding (or equivalent data over z') holding at the periphery $r' = r'_o$. Moreover, for consistency, (3.23) and the boundary conditions constrain $\eta'(r', z')$, so that, remarkably, even without finding the contour of any streamline $\eta'(r', z')$ within the bulk-vortex module I, we do know, but only to within the adequacy of the incompressible-boundary-layer dynamics, the (r', z'_{edge}) at which a particular streamline, entering the module I at (r'_o, z'), exits module I. Hence, setting aside the caveat, from the invariance of Y' and E' along streamlines, we know $E'(r', z'_{edge})$ and $Y'(r', z'_{edge})$. One algebraic detail: the streamfunction $\eta'(r', z')$ is a dependent variable, and hence we shall have no qualms about retaining the boundary-layer-motivated, diffusively characterized normalization for $\eta'(r', z')$ even for the inviscid bulk-vortex module I.

Formally for now, until the details are presented in § 4, we adopt placeholders $E'_{edge}(r')$, $Y'_{edge}(r')$, and write

$$E'(r', z'_{edge}) = E'_{edge}(r'), \tag{3.35}$$

$$Y'(r', z'_{edge}) = Y'_{edge}(r'). \tag{3.36}$$

If we non-dimensionalize consistently with (3.3) and (3.10), and adopt (the dimensionless stagnation energy $E(x, \zeta)$ is not to be confused with the Ekman number E)

$$E(x, \zeta) = E'(r', z')/c'_p T'_{amb,s} \approx T'(r', z')/T'_{amb,s} + \pi_1 Y'(r', z')/Y_{amb,s}, \tag{3.37a}$$

$$\pi_1 \equiv L' Y_{amb,s}/c'_p T'_{amb,s}, \tag{3.37b}$$

$$Y(x, \zeta) = Y'(r', z')/Y_{amb,s}, \tag{3.38}$$

then with $\phi(x, \zeta)$ and $w(x, \zeta)$ in hand from § 3.1,

$$\phi E_x + w E_\zeta = E_{\zeta\zeta}, \quad \phi Y_x + w Y_\zeta = Y_{\zeta\zeta}. \tag{3.39a,b}$$

If in (3.28), as compensation for ignoring the vortex-induced ocean-surface-temperature fall with decreasing radius, we also ignore surface-pressure fall with decreasing radius – both readily relaxed approximations – the boundary conditions become

$$E(x, 0) = 1 + \pi_1, \quad Y(x, 0) = 1; \tag{3.40}$$

$$E(1, \zeta) = T'_{amb}(z')/T'_{amb,s} + \pi_1 Y'_{amb}(z')/Y_{amb,s}, \tag{3.41}$$

$$Y(1, \zeta) = Y'_{amb}(z')/Y_{amb,s}, \tag{3.42}$$

where it is recalled that $\zeta = (z'/r'_o)/(E/2)^{1/2} = z'/(\nu'/2\Omega')^{1/2}$;

$$E(x, \zeta \to \zeta_{edge}) \to E'_{edge}(r')/(c'_p T'_{amb,s}), \tag{3.43}$$

$$Y(x, \zeta \to \zeta_{edge}) \to Y'_{edge}(r')/Y_{amb,s}, \tag{3.44}$$

where it is recalled that $x = r'^2/r_o'^2$. Again, numerically, we apply (3.43) and (3.44) at $\zeta = 5$, which is equivalent to a physical altitude of 1 km, for the adopted value of ν' and a pertinent value of Ω'.

Results are presented in § 4.1, after the functions $E'_{edge}(r')$ and $Y'_{edge}(r')$ in (3.43) and (3.44) are derived from inputs.

4. The dynamics and energetics of the bulk-vortex module

4.1. *Formulation for the bulk-vortex module*

Following Batchelor (1967), Battaglia, Rehm & Baum (2000), and Howard Baum (2005; unpublished), the dimensional equations for the steady axisymmetric inviscid swirling flow in the bulk-vortex module I, are examined in the non-inertial frame of reference and with the cylindrical polar coordinates previously adopted for the boundary-layer module. However, the greater vertical extent of the bulk vortex requires explicit accounting for density changes in discussing the module. Thus, we reformulate:

$$\partial(\rho' u' r')/\partial r' + \partial(\rho' w' r')/\partial z' = 0 \Rightarrow \partial\eta'/\partial r' = \rho' w' r', \quad \partial\eta'/\partial z' = -\rho' u' r'; \tag{4.1}$$

$$(u'\partial/\partial r' + w'\partial/\partial z')(r'v' + \Omega' r'^2) = 0 \Rightarrow r'v' + \Omega' r'^2 = \Gamma'(\eta') \rightarrow \Gamma'_o, \tag{4.2}$$

where Γ'_o is a constant for the (previously discussed) special but practically important case of a generalized potential vortex, in which the angular momentum is the same on all streamlines. In the absence of radiative effects,

$$(u'\partial/\partial r' + w'\partial/\partial z')(c'_p T' + L'Y' + g'z' + q'^2/2) = 0$$

$$\Rightarrow c'_p T' + L'Y' + g'z' + q'^2/2 = E'(\eta'). \tag{4.3}$$

If $\dot{m}'(r', z')$ denotes the rate at which water-vapour mass is condensed per unit mass, then

$$(u'\partial/\partial r' + w'\partial/\partial z')Y' = -\dot{m}' \Rightarrow Y' = Y'(\eta'), \tag{4.4}$$

if $\dot{m}' \approx 0$ in the unsaturated bulk vortex.

In the absence of mechanical dissipation, diffusion, and radiation, the entropy satisfies (e.g. Goldstein 1960)

$$(u'\partial/\partial r' + w'\partial/\partial z')S' = 0 \Rightarrow S' = S'(\eta'), \tag{4.5}$$

where $T'\,\mathrm{d}S' = c'_p\,\mathrm{d}T' - (1/\rho')\,\mathrm{d}p'$ in the absence of saturation and condensation, so with $p' \approx \rho' R'_a T'$,

$$p'/p'_{ref} = (T'/T'_{ref})^{\gamma/(\gamma-1)} \exp[-S'(\eta')/R'_a]$$

$$\Leftrightarrow S'(\eta')/R'_a = [\gamma/(\gamma-1)]\log(T'/T'_{ref}) - \log(p'/p'_{ref}), \tag{4.6}$$

where p'_{ref}, T'_{ref} are reference values to be assigned. From (4.3), (4.6), and the equation of state,

$$\rho'/\rho'_{ref} = \{[E'(\eta') - L'Y'(\eta') - g'z' - (q'^2/2)]^{1/(\gamma-1)}/c'_p T'_{ref}\}\exp[-S'(\eta')/R'_a]. \tag{4.7}$$

Hence, once the streamfunction $\eta'(r', z')$ is known within the bulk vortex, all physical variables may be found in that module, without iteration, as simple algebraic functions of $[r', z', \eta'(r', z')]$, since $E'(\eta')$, $Y'(\eta')$, $S'(\eta')$, and Γ'_o are regarded as identified from conditions specified at the peripheral boundary of the bulk-vortex module I. An equation for $\eta'(r', z')$ is derived in the Appendix, but, in fact, (4.1)–(4.7) suffice for our purposes.

4.2. *Boundaries and boundary conditions: the bulk-vortex/boundary-layer interface and the periphery*

A Dirichlet condition specifies the value of $\eta'(r', z')$ on the boundary of the bulk-vortex module I (figure 1). The boundary consists of three segments: (i) the planar interface with the underlying boundary layer, on which $\eta'(r', z'_{edge})$ is to be specified for $r'_{min} \leqslant r' \leqslant r'_o$; (ii) the periphery, on which $\eta'(r'_o, z')$ is to be specified for $z'_{edge} \leqslant z' \leqslant z'_{interface}$; and (iii) a yet-to-be-delineated segment of a streamline that demarcates the interface between the inviscid bulk vortex I and the inviscid core III, the continuous segment extending from (r'_{min}, z'_{edge}) to $(r'_o, z'_{interface})$. The altitude $z'_{interface}$ at the periphery distinguishes altitudes of inflow to the vortex, $0 \leqslant z' \leqslant z'_{interface}$, from altitudes of efflux from the vortex, $z'_{interface} \leqslant z' \leqslant z'_{lid}$, with z'_{lid} denoting the top of the vortex. The radius r'_{min} along the bulk-vortex/boundary-layer interface distinguishes radii of downflux to the boundary layer, $r'_{min} \leqslant r' \leqslant r'_o$, from radii of efflux from the boundary layer, $0 \leqslant r' \leqslant r'_{min}$. Alternatively, the radius r'_{min} may be described as the radius at which the boundary layer separates. The transitions at $z'_{interface}$ and r'_{min} might be either abrupt or gradual.

The approach adopted here (§ 2.2) is that trial values of $z'_{interface}$ and r'_{min} are adopted, and the existence, uniqueness, and stability of vortex solutions then explored. Choice of $z'_{interface}$ relates to the moisture content and speed of influx to the bulk vortex, while choice of r'_{min} relates to how much spinup from the ambient value v'_o occurs under conservation of angular momentum. This approach seems to us to be distinguished from the inverse procedure of assigning both the magnitude of the peak relative swirl and the radius at which it occurs, and of then ascertaining an ambient in which the pair of assignments could arise.

At the planar interface of the bulk vortex with the underlying boundary layer, $z' = z'_{edge}$, with the dimensionless downdrift $W(x; \varepsilon)$ defined below (3.18) and with $\rho' \to \rho'_{ref}$ to accommodate the incompressible treatment of the boundary layer, then (§ 3.1)

$$\eta'(r', z'_{edge}) = \rho'_{ref} \Omega' r'^3_o (E/2)^{1/2} \int_1^x W(y; \varepsilon)\, \mathrm{d}y, \quad x_{min} \leqslant x \leqslant 1, \tag{4.8}$$

where $x = r'^2/r'^2_o$ from (3.10). Since $W(x; \varepsilon) < 0$ over the radial expanse under study, then the peak value $\eta'_{max} = \eta'(r'_{min}, z'_{edge})$. This is the throughput, in mass/time, processed in the vortex. We may also define from (4.8) the inverse function $r'(\eta', z'_{edge})$.

At the periphery $r' = r'_o$, with $u'(r'_o, z')$ denoted $u'_{in}(z')$ and with $\eta'(r'_o, z'_{edge}) \approx 0$,

$$\eta'(r'_o, z') = -r'_o \int_{z'_{edge}}^{z'} \rho'(\bar{z}) u'_{in}(\bar{z})\, \mathrm{d}\bar{z}, \quad z'_{edge} \leqslant z' \leqslant z'_{interface}. \tag{4.9}$$

For self-consistency, the inflow $u'_{in}(z')$ is constrained by $\eta'(r'_o, z'_{interface}) = \eta'_{max}$. For the case $u'_{in}(z')$ const, by use of (3.34) and the definition of η'_{max}, the inflow

$$-u'_{in} = \left[\rho'_{ref} g' r'^2_o (E/2)^{1/2} \int_1^{x_{min}} W(y; \varepsilon)\, \mathrm{d}y \right] / [p'(r'_o, z'_{edge}) - p'(r'_o, z'_{interface})]. \tag{4.10}$$

More importantly, from (3.34) and (4.8)–(4.10),

$$\eta'(r'_o, z')/\eta'_{max} = \left[p'(r'_o, z'_{edge}) - p'(r'_o, z')\right] / \left[p'(r'_o, z'_{edge}) - p'(r'_o, z'_{interface})\right]. \tag{4.11}$$

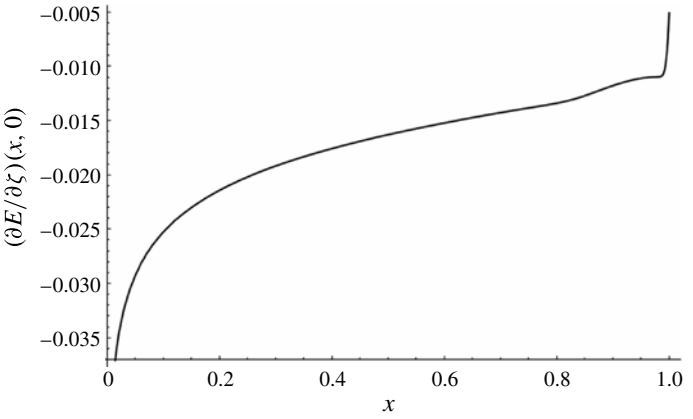

FIGURE 13. For the case presented in figure 5, the normalized gradient of the total stagnation energy (defined dimensionally in (3.25) and non-dimensionally in (3.37)) at the nominal air/sea interface, $E_\zeta(x, 0)$, versus x, for a scenario with $E(1, \zeta)$, $E(x, 0)$, and $E(x, \zeta_{edge})$ as depicted in figure 15. The boundary-layer-top-edge profiles $E(x, \zeta_{edge})$ and $Y(x, \zeta_{edge})$ are correlated with the Jordan mean ambient for the autumnal maritime tropics, taken to hold at the periphery, $r = 1$ (§ 4.2). Here, $\varepsilon = 10^{-3}$, $r_{min} = 0.118$, $z_{edge} = 0.076$, and $z_{interface} = 0.249$, where $x_{min} = r_{min}^2$, the radial coordinate is normalized by $r'_o (= 339\ \text{km})$, and the axial coordinate is normalized by $z'_{lid} (= 12.7\ \text{km})$. A uniform inflow $u_{in} = -0.704$ over the vertical span $(z_{edge}, z_{interface})$ is adopted at the periphery (see (4.10)), velocities being normalized by $\Omega' r'_o = 5.90\ \text{m s}^{-1}$.

From the thermodynamic data holding at the periphery $r' = r'_o$, the values of the three energetics-related integrals holding on the streamlines in the bulk vortex $S'_{bv}(r'_o, z')$, $Y'_{bv}(r'_o, z')$, and $E'_{bv}(r'_o, z')$ may be computed with the use of (3.31)–(3.33), (4.2)–(4.4), and (4.6). From the inverse function $z'(r'_o, \eta')$ implicitly defined by (4.11), the three integrals $S'_{bv}\left[\eta'(r'_o, z')\right]$, $Y'_{bv}\left[\eta'(r'_o, z')\right]$, and $E'_{bv}\left[\eta'(r'_o, z')\right]$ are in hand. The general function $\eta'(r', z')$ is neither known nor needed, because our boundary-layer-focused requirements are met by (4.8) and (4.9), which link $r'(\eta', z'_{edge})$ and $z'(r'_o, \eta')$. For the purpose of (3.43) and (3.44), since we have the correlation between $\eta'(r'_o, z')$ and $\eta'(r', z'_{edge})$:

$$E'_{edge}(r') = E'_{bv}\left[\eta'(r', z'_{edge})\right], \quad Y'_{edge}(r') = Y'_{bv}\left[\eta'(r', z'_{edge})\right]. \tag{4.12}$$

For completeness, $S'_{edge}(r') = S'_{bv}[\eta'(r', z'_{edge})]$.

With the formulation in (3.37)–(3.44) now completed, the sea–air transfers $E_\zeta(x, 0)$ and $Y_\zeta(x, 0)$ may be calculated (figures 13 and 14) as well as profiles of $E(x, \zeta)$ and $Y'(x, \zeta)$ (figures 15 and 16). The convectively unstable stratification with altitude of the autumnal maritime tropical ambient is reflected in the radial variation of the total stagnation energy E at the top edge of the boundary layer (figure 15). This convectively unstable stratification of E is due principally to the monotonic decrease of the water-vapour mass fraction Y' with altitude in the ambient, a distribution also reflected in the radial distribution at the top edge of the boundary layer (figure 16). However, a likely corresponding decrease of E, again due to a decrease of Y' with decreasing radial position at the sea surface, has been ignored, in that the sea-surface temperature under the vortex has been idealized as radially invariant. Hence, the increase (in magnitude of the sea-to-air transfer) with decreasing radii is likely to be

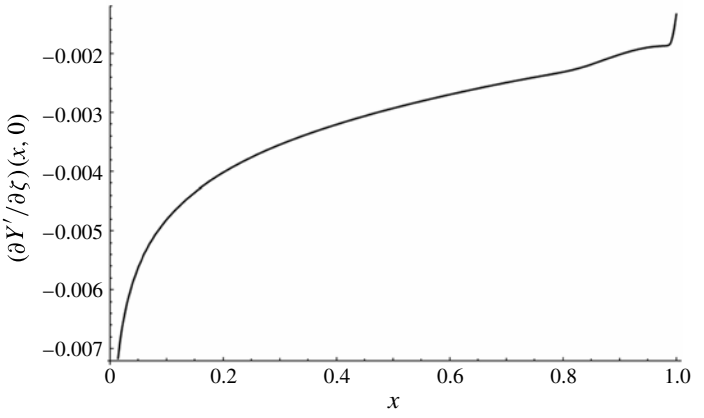

FIGURE 14. For the case presented in figure 13, the gradient of the water-vapour mass fraction (defined in (3.31)) at the nominal sea–air interface, $Y'_\zeta(x, 0)$, versus x, with $Y'(1, \zeta)$, $Y'(x, 0)$, and $Y'(x, \zeta_{edge})$ as depicted in figure 16. No account is taken here, or in figure 13, of the cooling of the ocean surface induced by a well-organized atmospheric vortex. Even so, the magnitude of the enhancement in sea-to-air transfer within the vortex remains modest.

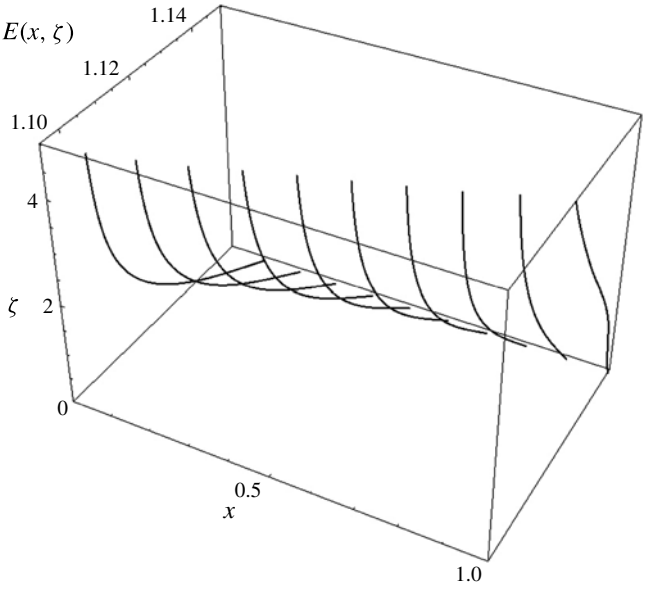

FIGURE 15. For the case presented in figure 13, profiles of the normalized total stagnation energy $E(x, \zeta)$ versus ζ at ten uniformly spaced values of the streamwise coordinate x spanning the range (0.1, 1.0).

less than that depicted in figures 13 and 14. Moreover, taking into account, while holding invariant the total throughput rate η'_{max}, that the inflow at the periphery $u'_{min}(z')$ probably is non-uniform and plausibly decreases monotonically in magnitude with increasing axial position z', also modifies the radial distribution of E and Y' at the top

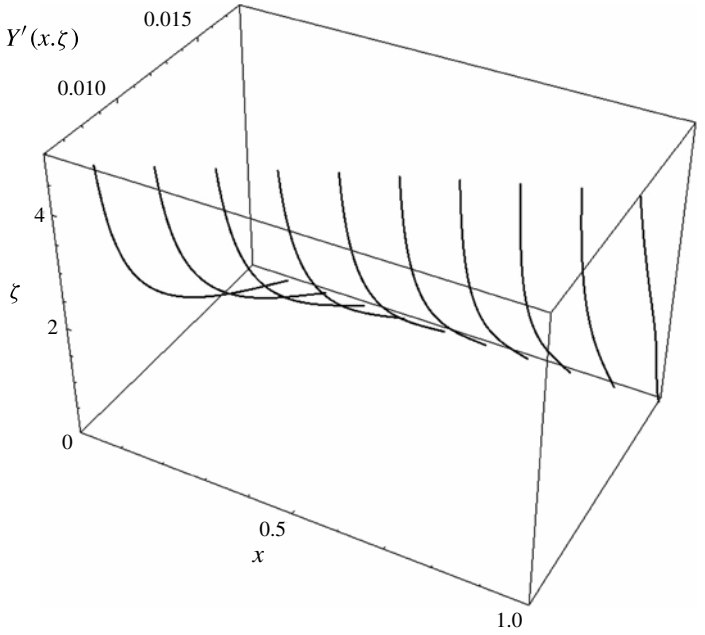

FIGURE 16. For the case presented in figure 13, profiles of the water-vapour mass fraction $Y'(x, \zeta)$ versus ζ at ten uniformly spaced values of the streamwise coordinate x spanning the range (0.1,1.0).

edge of the boundary layer, such that the magnitude of the sea-to air transfer would decrease at most radii.

In the light of recent suggestions (Zhang & Drennan 2012), we found a modest change in results from our model from letting: the Prandtl number be 1.6, rather than unity, on the right-hand side of (3.39*a*); the Schmidt number be 0.9, rather than unity, on the right-hand side of (3.39*b*); and, in both equations, the eddy viscosity decrease monotonically with increasing ζ, from a maximum value at $\zeta = 0$ to zero at the top edge, rather than remaining invariant across the boundary-layer thickness.

4.3. *Boundaries and boundary conditions: the bulk-vortex/core interface*

At the interface between the bulk vortex and the core, from (r'_{min}, z'_{edge}) to $(r'_o, z'_{interface})$, lies the 'streamline' $\eta' = \eta'_{max}$. A task is to deduce the position of, and properties along, the interface from a reasonable set of physical approximations. Executing the steps has not proved necessary to elucidate the boundary-layer dynamics and energetics, the focus of this paper. But with the boundary-layer dynamics and energetics in hand, execution both ensures that the model underlying the boundary-layer treatment admits a physically consistent solution, and provides the geometry for subsequent studies of the core module III. From the thermodynamic data and relative swirl holding at the periphery, good approximations to the values of the four integrals holding all along the streamline on the bulk-vortex side of the interface $S'_{bv}(\eta'_{max})$, $Y'_{bv}(\eta'_{max})$, $E'_{bv}(\eta'_{max})$, and $\Gamma'_{bv}(\eta'_{max}) = \Gamma'_o$ may be computed with the use of (3.31)–(3.34), (4.2), (4.3), (4.6), and (3.20). The pressure is also known on the bulk-vortex side of the interface at $(r'_o, z'_{interface})$ from the thermodynamic data at the periphery, and this value of the pressure holds on the core-module side at $(r'_o, z'_{interface})$ as well, since the pressure is continuous across the interface. The pressure

at (r'_{min}, z'_{edge}) is obtained from integration at $z' \approx z'_{edge}$ of the differential equation (3.7), generalized to admit variable density, and (3.20). The variable density is available from a combination of (4.7), (4.12), the relation just after (4.12), the polynomial curve fit to figure 4, and the approximation $q' \to v'$. Admittedly, the accuracy with which the radial distribution of this density is known is compromised by approximations, as discussed in § 3.2. A boundary condition for the integration, the pressure $p'(r'_o, z'_{edge})$, is available from the thermodynamic data at the periphery. Again, the same pressure holds on the bulk-vortex and core side at (r'_{min}, z'_{edge}) as well.

On the saturated, core side of the interface, $\dot{m}' > 0$ in (4.4), and $Y' \to Y'_s$:

$$(u'\partial/\partial x' + w'\partial/\partial z')Y'_s = \dot{m}' \Rightarrow Y'_{core} = Y'_s = \sigma P'(T')/p'. \tag{4.13}$$

Equation (4.3) continues to hold, but in the light of (4.13), and if the approximation $q'^2 \to v'^2$ is again adopted,

$$c'_p T'_{core} + L' Y'_s(T'_{core}, p') + g'z' + v'^2/2 = E'_{core}(\eta'_{max}). \tag{4.14}$$

In the core module III, the entropy is again constant on streamlines, as stated in (4.5), but now the second law is modified to account for saturation and condensation (Houghton 1986), so the expression for the entropy is, in turn, modified:

$$p'/p'_{ref} = (T'_{core}/T'_{ref})^{\gamma/(\gamma-1)} \exp\left\{-[S'_{core}(\eta'_{max})]/R'_a + L' Y'_s(T'_{core}, p')/R'_a T'_{core}\right\} \Longleftrightarrow$$
$$S'_{core}(\eta'_{max}) = c'_p \log(T'_{core}/T'_{ref}) - R'_a \log(p'/p'_{ref}) + L' Y'_s(T'_{core}, p')/T'_{core}. \tag{4.15}$$

Equation (4.2) holds in the inviscid core, so the absolute angular momentum is constant on streamlines, but may be expected to vary from streamline to streamline in the core. However, as noted earlier (§ 2.3), the swirl v' is taken to be continuous across the interface between modules I and III. Thus,

$$r'v' + \Omega' r'^2 = \Gamma'_o \Longleftrightarrow v' = (\Gamma'_o - \Omega' r'^2)/r' \tag{4.16}$$

holds on the core-side streamline, as well as on the bulk-vortex-side streamline, of the interface.

It is recalled that the pressure is continuous across the interface, and $E'_{core}(\eta'_{max})$ and $S'_{core}(\eta'_{max})$ are each constant all along the streamline on the core side of the interface.

Accordingly, evaluating (4.14) and (4.15), together with (4.13), at (r'_{min}, z'_{edge}) and $(r'_o, z'_{interface})$, provide four simultaneous nonlinear algebraic equations for the four interface-related unknowns:

$T'_{core,bottom}$, the temperature for a site just to the core side (of the bulk-vortex/core interface) at the base of the interface (i.e. at (r'_{min}, z'_{edge}));

$T'_{core,top}$, the temperature for a site just to the core side at the top of the interface (i.e. at $(r'_o, z'_{interface})$);

$E'_{core}(\eta'_{max}) \equiv E'_{core,interface}$, the total stagnation energy at all sites just to the core side of the interface, which is the 'streamline' with the highest value (if the sea surface is the streamline datum, here taken as null value); and

$S'_{core}(\eta'_{max}) \equiv S'_{core,interface}$, the entropy at all sites just to the core side of the interface, the core being saturated throughout (while the bulk vortex is unsaturated throughout), in a time-averaged description.

The four relations are ($T'_{ref} = T'_{amb,s}$, $p'_{ref} = p'_{amb,s}$ being convenient choices):

$$c'_p T'_{core,bottom} + L'\sigma P'(T'_{core,bottom})/p'_{interface,bottom} + g' z'_{edge} + v'^2(r'_{min})/2 = E'_{core,interface}; \tag{4.17}$$

$$c'_p\ T'_{core,top} + L'\sigma P'(T'_{core,top})/p'_{interface,top} + g' z'_{interface} + v'^2(r'_o)/2 = E'_{core,interface}; \tag{4.18}$$

$$c'_p \log(T'_{core,bottom}/T'_{ref}) - R'_a \log(P'_{interface,bottom}/p'_{ref}) + L'\sigma P'(T'_{core,bottom})/T'_{core,bottom} p'_{interface,bottom} = S'_{core,interface}; \tag{4.19}$$

$$c'_p \log(T'_{core,top}/T'_{ref}) - R'_a \log(P'_{interface,top}/p'_{ref}) + L'\sigma P'(T'_{core,top})/T'_{core,top} p'_{interface,top} = S'_{core,interface}. \tag{4.20}$$

With $E'_{core}(\eta'_{max})$ and $S'_{core}(\eta'_{max})$ in hand, to complement $S'_{bv}(\eta'_{max})$, $Y'_{bv}(\eta'_{max})$, $E'_{bv}(\eta'_{max})$, and $\Gamma'_{bv}(\eta'_{max}) = \Gamma'_o$, enforcement, at general sites along the interface streamline, of continuity of pressure across the interface streamline is achieved by equating the expressions for pressure on the core side, (4.15), and for pressure on the bulk-vortex side, (4.6). For any value of pressure in the range ($p'_{interface,bottom}$, $p'_{interface,top}$), the associated pair of coordinates (r', z') along the interface may be found by solution of three simultaneous nonlinear coupled algebraic equations. The task involves three relations because T'_{core} along the interface on the saturated, core side, and thus (4.14), becomes inextricably enmeshed in the calculation (whereas the temperature T' along the interface on the unsaturated, bulk-vortex side can be eliminated by (4.3)).

For the Jordan ambient and adopted values for the interface-end-'points' parameters r'_{min} and $z'_{interface}$, results computed for the four interface-related unknowns, listed above (4.17) and generated by solution of (4.17)–(4.20), are given in table 2. Standard iterative methods suffice for solving these four simultaneous nonlinear algebraic equations. More advanced, cost-function-based methods are used to generate the (r, z) contours for the interface between the bulk-vortex and core modules from solution of the coupled nonlinear equations (4.6), (4.14), and (4.15) (figures 17 and 18); $r = r'/r'_o$, $z = z'/z'_{lid}$. The difference in axial span (a few kilometres) and radial span (a few hundred kilometres) in figures 17 and 18 is emphasized.

While the recent advent of overflights by multiply-instrumented, high-altitude, long-endurance, remotely piloted aeronautical systems may afford sustained monitoring, to date there has been limited measurement to provide time-averaged, highly vertically resolved thermohydrodynamic structure of a tropical cyclone. Figures 17 and 18, together with table 2, suggest that, for most radii, the interface between upper-tropospheric efflux and lower tropospheric influx could be at lower altitude (higher pressure) than sometimes conjectured.

5. The boundary-layer-corner flow

The dynamics and energetics in the relatively small portion of the boundary-layer module II from which fluid is detrained, at an (evidently) relatively rapid rate, and which is referred to as the 'corner' of the boundary layer, are now addressed. This corner of the boundary layer, in which a swirling inflow is turned into a swirling updraft, may be characterized, rather arbitrarily, as occupying, in general, $0 \leqslant x \leqslant x_{min}$, $0 \leqslant \zeta \leqslant \zeta_{edge} (\simeq 5)$. Attention in this section is focused on a tropical-storm-intensity vortex (figure 1), rather than a more intense vortex in which an eye may descend to sea level (figure 2). Treatment of a separating boundary layer entails approximation,

Scenario		Results			
r'_{min} (km)	$z'_{interface}$ (km)	$T'_{core,bottom}$ (K)	$T'_{core,top}$ (K)	$E'_{core}(\eta'_{max})$ (kJ kg^{-1})	$S'_{core}(\eta'_{max})$ (J (kg K)$^{-1}$)
40	4.42	283.7	265.3	318.2	62.9
40	3.77	283.3	268.9	317.2	59.5
40	3.16	282.9	271.9	316.2	56.2
40	2.59	283.5	274.6	315.2	53.8
40	2.05	283.1	277.2	314.3	49.8
20	3.16	279.7	270.5	313.4	46.1
30	3.16	282.1	271.6	315.5	53.8
40	3.16	282.9	271.9	316.2	56.2
50	3.16	283.3	273.0	316.4	57.2
60	3.16	283.5	272.1	316.5	57.7

TABLE 2. Properties holding on the core side of the interface between the bulk-vortex and core modules, for several selected scenarios. (Note: All results are based on the Jordan ambient in table 1, for a potential vortex (4.16), with the pressure at the bottom (base) of the interface calculated from (3.7), generalized to encompass variable density, and (3.20). Nominal parameters assignment ($r'_o = 300$ km, $z'_{edge} = 1$ km, $\epsilon = 10^{-3}, \ldots$) hold. The reference for entropy is implicit in (4.15).)

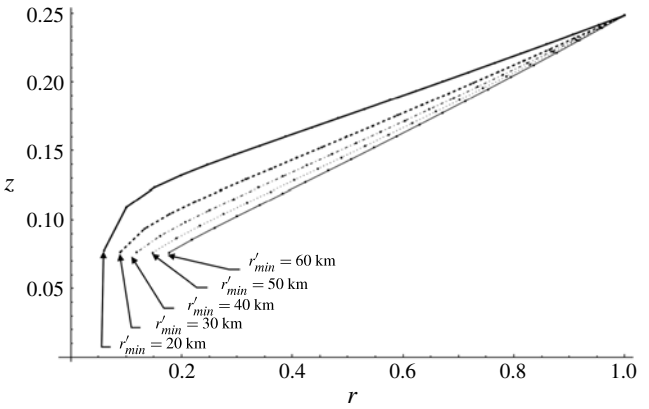

FIGURE 17. Contours of the streamline/vortex-sheet/contact-surface interface between the bulk-vortex module I and the core module III in dimensionless (r, z) coordinates, with $r = r'/r'_o$, where peripheral radius $r'_o = 300$ km; and $z = z'/z'_{lid}$, where the 'lid' height $z'_{lid} = 12.7$ km. The interface spans the end 'points' (r_{min}, z_{edge}) and $(1, z_{interface})$. Here, the thickness of the boundary layer z_{edge}, and the altitude separating influx and efflux at the periphery $z_{interface}$, are held fixed, and the contours hold for various values of the radius of boundary-layer separation, $r_{min} = r'_{min}/r'_o$. The Jordan mean ambient for the autumnal maritime tropics holds at the periphery.

and here the corner flow is regarded tentatively as an inviscid locale in which unsaturated, but relatively warm and moist, air enters at (x_{min}, ζ) for $0 \leqslant \zeta \leqslant \zeta_{edge}$, and saturated air exits at (x, ζ_{edge}) for $0 \leqslant x \leqslant x_{min}$. Of course, in fact, the corner flow is not inviscid, and eventual modification of this convenient oversimplification is anticipated. Alternative postulates for facile treatment of the corner flow seem comparably moot.

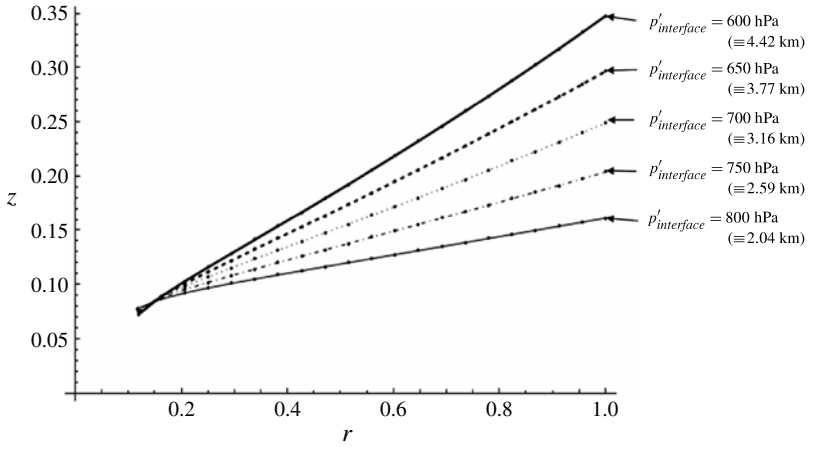

FIGURE 18. Contours of the interface described in figure 17, but here the radius of the boundary-layer separation, r'_{min} is held fixed at 40 km, the boundary-layer thickness z'_{edge} is held fixed at 1 km, and the contours hold for various values of the altitude marking transition between influx and efflux at the periphery, $z_{interface}(\equiv z'_{interface}/z'_{lid})$. Values of $z'_{interface}$ are listed in parentheses, along with values of the associated pressure $p'_{interface}$.

Accordingly, just as the invariance of integrals along streamlines was exploited to correlate properties at the periphery of the inviscid bulk-vortex module with properties at the entraining edge of the boundary layer, so again the invariance of integrals along streamlines is exploited to correlate ζ-dependent properties at $x = x_{min}$ to x-dependent properties at $\zeta = \zeta_{edge}$. Once again there is no need to delve into streamline configuration within the turning-flow domain. For the corner flow, with onset of saturation and condensation, the three invariant integrals are absolute angular momentum Γ, the total stagnation energy E, and the entropy S. In general, the value of each integral, while invariant along streamlines, varies from streamline to streamline.

At $x = x_{min}$, with the streamfunction $\eta(x, \zeta)$, non-dimensionalized by $\rho'_{ref}\Omega' r'^3_o (E/2)^{1/2}$, where E denotes the Ekman number, then, from (3.23), over the range $0 \leqslant \zeta \leqslant \zeta_{edge}$,

$$\partial\eta(x_{min}, \zeta)/\partial\zeta = -\phi(x_{min}, \zeta), \quad \eta(x_{min}, 0) = 0, \tag{5.1}$$

with $\phi(x_{min}, \zeta)$ in hand (§ 3.1). As noted at the start of § 4.3, $\eta(x_{min}, \zeta_{edge}) = \eta_{max}$.

Thus, if the entropy is non-dimensionalized against R'_a, T' is non-dimensionalized against $T'_{amb,s}$, and $z' = (\nu'/2\Omega')^{1/2}\zeta$,

$$\Gamma(x_{min}, \zeta) = \psi(x_{min}, \zeta) + x_{min}, \quad v(x_{min}, \zeta) = \psi(x_{min}, \zeta)/x_{min}^{1/2}, \tag{5.2a,b}$$

$$E(x_{min}, \zeta) \approx T(x_{min}, \zeta) + \pi_1 Y(x_{min}, \zeta), \tag{5.3}$$

$$S(x_{min}, \zeta) = [\gamma/(\gamma - 1)] \log T - \log\{[p'_{interface,bottom} + \rho'_{ave} g'(z'_{edge} - z')]/p'_{amb,s}\}. \tag{5.4}$$

Typically at separation, x_{min} is a relatively small contributor on the right-hand side of (5.2a). It is recalled that the variable Y in (5.3) is normalized in accord with (3.38). In particular, $\Gamma(x_{min}, \zeta_{edge}) = 1 + \varepsilon$, for self-consistency. Hence, by change of variable, $\Gamma_{b\ell}[\eta(x_{min}, \zeta)]$, and $S_{b\ell}[\eta(x_{min}, \zeta)]$ are in hand.

At $z' = z'_{edge}$, $w(x, \zeta_{edge}; \varepsilon) = w_{out}(x; \varepsilon) = W(x; \varepsilon)$, where $W(x; \varepsilon) \geqslant 0$ over the range of interest, $0 \leqslant x \leqslant x_{min}$:

$$\eta(x, \zeta_{edge}) \equiv \eta_{edge}(x) = \eta_{max} - \int_x^{x_{min}} W(y; \varepsilon)\, \mathrm{d}y, \quad \eta(0, \zeta_{edge}) = 0, \tag{5.5}$$

from (3.23) and (5.1). For the special case $W(y; \varepsilon)$ const,

$$W = \eta_{max}/x_{min}, \quad 0 \leqslant x \leqslant x_{min} \quad \text{and} \quad \eta(x, \zeta_{edge}) = \eta_{edge}(x) = \eta_{max}(x/x_{min}). \tag{5.6}$$

We have the correlation between $\eta(x_{min}, \zeta)$ and $\eta(x, \zeta_{edge}) = \eta_{edge}(x)$. Hence, at $\zeta = \zeta_{edge}$ for $0 \leqslant x \leqslant x_{min}$, the three integrals, in dimensionless presentation, are as follows. First, denoting $v(r, \zeta_{edge}) \equiv v_{edge}(r)$,

$$rv_{edge} + r^2 = \Gamma_{edge}(r) = \Gamma_{b\ell}[\eta(x, \zeta_{edge})]. \tag{5.7}$$

Second, the temperature is non-dimensionalized against $T'_{amb,s}$, and the saturation water-vapour mass fraction (given by (4.13)) is normalized against $Y_{amb,s}$, as was done in (3.37) and (3.38). Then, discarding the subscript *edge* on T and p,

$$T + \pi_1 Y_s(T, p) \simeq E_{edge}(r) = E_{b\ell}\left[\eta(x, \zeta_{edge})\right]. \tag{5.8}$$

Third, with the entropy non-dimensionalized against R'_a,

$$\log[T^{\gamma/(\gamma-1)}/p] + [\gamma/(\gamma - 1)]\pi_1 Y_s(T, p)/T = S_{edge}(r) = S_{bl}[\eta(x, \zeta_{edge})]. \tag{5.9}$$

Equations (5.8) and (5.9) are two coupled nonlinear algebraic equations for $T(r)$ and $p(r)$, over $0 \leqslant r \leqslant r_{min}$ at $\zeta = \zeta_{edge}$. The other state variables may be found over the same range, without iteration, from the relations (3.31)–(3.33).

In (5.8), $E_{b\ell}[\eta(x \to x_{min}, \zeta_{edge})] \to E_{b\ell}(\eta_{max})$, whereas $E_{b\ell}[\eta(x \to x_{min}, \zeta_{edge})] \to E_{core}(\eta_{max})$ is appropriate. In (5.9), $S_{b\ell}[\eta(x \to x_{min}, \zeta_{edge})] \to S_{b\ell}(\eta_{max})$, whereas $S_{b\ell}[\eta(x \to x_{min}, \zeta_{edge})] \to S_{core}(\eta_{max})$ is appropriate. Such local *ad hoc* smoothing to account for transfer of properties across streamlines in diffusive corner flow seems no more arbitrary than postulating other radial profiles of $E'_{edge}(r')$ and $S'_{edge}(r')$, or equivalent statements, at the exit from the corner flow.

6. Discussion; future agenda

Most models undertaking high-resolution treatment of the tropical-cyclone boundary layer seek to isolate that module from the remainder of the vortex structure. This, of course, is precisely the opposite of the emphasis on modular interconnectedness of the approach undertaken here, which has the ultimate goal of a composite description. Nevertheless, brief juxtaposition with selected examples of other works is undertaken, without any attempt at a complete literature survey.

Kepert (2010) has contrasted his direct-numerical-integration results for an unsteady three-dimensional (in practice, often axisymmetric) mixing-length/gradient-diffusion (parabolic) model of a tropical-cyclone boundary layer, with results obtained by Smith & Montgomery (2008) and Smith & Vogl (2008) for a roughly comparable (but steady-state axisymmetric) model via integration of ordinary differential equations after vertical averaging. Both approaches adopt constant density, and do not examine the thermodynamics of the boundary layer. For specificity, a stationary cyclone, with maximum azimuthal wind of 40 m s^{-1} at a radius of 40 km, is examined over an atmospheric domain that extends 40 km radially and 2 km vertically. Kepert takes issue with the overestimation of supergradient flow (flow in which the swirl at sites within the boundary layer achieves values exceeding the local boundary-layer-top-edge

swirl) that the slab treatment finds to be ubiquitously present, and also with the strong sensitivity to the Coriolis parameter inwards of 250 km manifested by the slab treatment. In contrast, a height-resolving solution shows only marginal supergradient flow, if it is present at all (in the cited scenario, the maximum azimuthal wind in the boundary layer is 43.2 m s^{-1} at a height of 400 m, an overshoot of only 6 %), and almost insensitivity to the Coriolis parameter in the core. In that our solution (as that of Burggraf *et al.* 1971, Carrier 1971*a*, and Carrier *et al.* 1994) thus far gives no hint of supergradient flow, and our solution reduces the role of the Coriolis parameter at smaller radii, our results to date side with Kepert's reservations. We do acknowledge that, near the top edge of the boundary layer at inner radial stations, swirl-velocity overshoot of its inviscid-flow asymptote has been observed to reach 10 % in laboratory experiment (Kendall 1962, pp. 8–9), and 15–25 % in at-sea dropwindsondes profiles (Sanger 2011; Black *et al.* 2012). Still, the discrepancy between profiles reported by dropwindsondes released in rapid succession and descending at 5–10 m s^{-1} raises issues regarding whether the profiles reflect instantaneous, not time-averaged, measurements in a highly unsteady flow field. In response to a conjecture of a reviewer, we have found that, in our model, admission of any amount of slip (at the nominal air/sea interface) of the azimuthal velocity component introduces no velocity overshoot anywhere in the boundary layer from the periphery to separation.

On the other hand, Kepert states that 'the slab model produces excessively strong inflow and too great departure of the boundary-layer mean winds from gradient balance' (p. 1689). Kepert describes efflux from the boundary layer out to a radius of 250 km, and a 'maximum inflow of 11 m s^{-1} at 60 m height and 60 km radius, or 1.5 times the RMW (radius of maximum winds)' (p. 1693). Here our results side with Smith and his cowokers in that we find that the strength of the low-level inflow speed in the boundary layer of an intense vortex can approach the swirl speed holding above the boundary layer at the same radial distance from the axis of the vortex, even though the magnitude of the velocity vector across most of the boundary layer does not depart greatly from the magnitude of the gradient wind. We also question that '…the higher-order closure is undoubtedly the more realistic of two…parameterizations…' (Kepert 2010, p. 1696) in that incorporation of more detail may introduce error as well as insight.

Even such brief juxtapositions suggest that our distinct perspective and results may usefully contribute to the efforts to elucidate the thermofluid-dynamics of tropical-cyclone structure.

While much additional parametric investigation of the results presented here would be useful, our next goal is to formulate and solve the quasi-linear second-order elliptical partial differential equation for the streamfunction in the inviscid saturated core (III) of a steady axisymmetric tropical storm (no eye). As suggested by our treatment of the core side of the core/bulk-vortex interface, we expect to bypass parameterization of cumulus convection and cloud microphysics. Nevertheless, by having the water-vapour mass fraction take on its saturated value at the local thermodynamic pressure and temperature, the partial differential equation for the streamfunction in the core is appreciably more intricate than that given in the Appendix for the unsaturated bulk vortex. A further complication is that the core module is bounded spatially by many 'segments': the axis of rotation; the 'lid'; the top of the boundary layer (as described in § 5); the curved interface (streamsurface) between the core and the bulk vortex; and the upper portion of the periphery of the domain. Moreover, in the core, expressing the local values of other dependent

variables in terms of the streamfunction entails iterative solution of coupled nonlinear algebraic equations giving the integrals for the angular momentum, entropy, and total stagnation energy. Efficient computation will be essential for parametric investigation. In terms of the interconnectedness of modules, in the absence of much mixing across streamlines in the corner flow of the boundary layer, we might expect moister, virtually non-rotating, rapidly streamwise-flowing air to ascend in the portion of the core closer to the axis, and drier, relatively rapidly rotating, less rapidly ascending air in the portion of the core further from the axis. The roughly rigid-body-like profile of the swirl in the inviscid core is a residual of friction acting in the boundary layer.

Eventually we aspire to address a more intense vortex, possessing a core with an eye (and thus a vortex with an eye–eyewall interface). The anticipations in the last paragraph seem consistent with a virtually non-rotating eye, sheared into recirculatory motion by contiguous eyewall updraft, with entrainment from the eyewall moistening the eye. The radially outwardly sloping eye/eyewall interface implies a longer column of compressionally heated, relatively light eye air overlying the portion of the eyewall air that ascends closer to the axis of rotation. However, air in this portion of the eyewall probably emerges from the boundary layer with relatively modest angular momentum. Thus, the lateral profiles of swirl and pressure within the lower-altitude eyewall will be interesting to study.

Acknowledgements

The work reported herein by F.F. was supported by Northrop Grumman Aerospace Systems. He is grateful to Leopold Andreoli for the opportunity to initiate this study, and to Ronald Polidan and Clark Snodgrass for the opportunity to complete it. He is grateful to Howard Baum of the University of Maryland for many helpful suggestions, including recommending the use of Mathematica, providing examples of Mathematica notebooks, suggesting the usefulness of the von Mises transformation for treating the dynamics of the boundary layer, and deriving (A 5)–(A 6).

Appendix. Derivation of an equation for the streamfunction in module I

The conservation of radial momentum for the steady inviscid axisymmetric flow in module I is, dimensionally,

$$\rho'(u'\partial u'/\partial r' + w'\partial u'/\partial z' - 2\Omega' v' - v'^2/r') + (\partial p'/\partial r')_{z'} = 0, \tag{A 1}$$

and is a convenient choice for deriving an equation for the streamfunction $\eta'(r', z')$. Since $p' = p'[r', z', \eta'(r', z')]$ according to (4.3)–(4.6),

$$(\partial p'/\partial r')_{z'} = (\partial p'/\partial \eta')_{r',z'}(\partial \eta'/\partial r')_{z'} + (\partial p'/\partial r')_{\eta',z'}. \tag{A 2}$$

With the aid of (4.6), (4.7), and the approximation $q'^2 \to v'^2$,

$$\begin{aligned}(\partial p'/\partial \eta')_{r',z'} = \rho'[&-T'\mathrm{d}S'(\eta')/\mathrm{d}\eta' + \mathrm{d}E'(\eta')/\mathrm{d}\eta' \\ &- L'\mathrm{d}Y'(\eta')/\mathrm{d}\eta' - v'(\partial v'/\partial \eta')_{r',z'}];\end{aligned} \tag{A 3}$$

also,

$$(\partial p'/\partial r')_{\eta',z'} = -\rho'[u'(\partial u'/\partial r')_{\eta',z'} + v'(\partial v'/\partial r')_{\eta',z'} + w'(\partial w'/\partial r')_{\eta',z'}]. \tag{A 4}$$

By substitution into (A 1), with ω'_θ denoting the azimuthal component of vorticity,

$$\begin{aligned}\omega'_\theta \equiv \partial u'/\partial z' - \partial w'/\partial r' = -\rho' r'[&-T'\mathrm{d}S'(\eta')/\mathrm{d}\eta' + \mathrm{d}E'(\eta')/\mathrm{d}\eta' \\ &- L'\mathrm{d}Y'(\eta')/\mathrm{d}\eta' - (v'/r')\mathrm{d}\Gamma'(\eta')/\mathrm{d}\eta'].\end{aligned} \tag{A 5}$$

For $\Gamma' = \Gamma'_o$ const, the right-hand side is a function of η' only, except for T', which is anticipated to vary by not much more than $\sim 5\,\%$ in the bulk vortex. Thus, the right-hand side is regarded approximately as a function of η' only. If that function of η' can be identified at any (r', z'), the identified function of η' holds at all (r', z') in the bulk vortex. By (4.1), the vorticity is related to the streamfunction, and a quasi-linear second-order elliptical partial differential equation for $\eta'(r', z')$ is obtained for the unsaturated module I:

$$\omega'_\theta = -\left\{(\partial/\partial z')[(1/\rho' r')\partial\eta'/\partial z'\right] + (\partial/\partial r')[(1/\rho' r')\partial\eta'/\partial r']\}. \tag{A 6}$$

For our purposes, the partial differential equations (A 5)–(A 6) need not be solved within the challengingly configured domain of module I. Nevertheless, some conjectures are made.

Substituting into the right-hand side of (A 5) for $\mathrm{d}E'(\eta')/\mathrm{d}\eta'$ from (4.3), with the $q'^2/2$ term neglected (see below (3.34)), and for $T'\mathrm{d}S'(\eta')/\mathrm{d}\eta'$ from (4.6), gives

$$\omega'_\theta = -\rho' r'(\mathrm{d}/\mathrm{d}\eta')\left(\int \mathrm{d}p'/\rho' + g' z'\right) \to 0 \tag{A 7}$$

under hydrostatics at $r' = r'_o$ where, by choice of the peripheral constraints, $\mathrm{d}(\ )/\mathrm{d}\eta' \to \partial(\ )/\partial z'$. Hence, ω'_θ is regarded approximately as zero in the bulk vortex, and (A 6) becomes a homogeneous equation for $\eta'(r', z')$. We may also argue that $\mathrm{d}(\ )/\mathrm{d}\eta' \to \partial(\ )/\partial z'$ at any r in the bulk-vortex module since the streamlines are everywhere nearly horizontal for the slab-like geometry of module I. Thus, by taking hydrostatics to hold, approximately, throughout module I, the argument for the vanishing of the terms in square brackets in (A 5) applies broadly. Then, by 'lagging' the dependence on the streamfunction η' of the density ρ', iterative solution of a linear elliptic second-order equation subject to Dirichlet boundary conditions, albeit with a curvilinear boundary segment, gives the streamfunction in the bulk-vortex module I.

REFERENCES

BATCHELOR, G. K. 1967 *An Introduction to Fluid Dynamics*, pp. 543–559. Cambridge University Press.

BATTAGLIA, F., REHM, R. G. & BAUM, H. R. 2000 The fluid mechanics of fire whirls: an inviscid model. *Phys. Fluids* **12**, 2859–2867.

BAUM, H. & FENDELL, F. 2006*a* HIRWG (Hurricane Intensity Research Working Group) minority report, 25 pp. http://www.sab.noaa.gov/Reports/HIRWG_finalMinority.pdf.

BAUM, H. R. & FENDELL, F. 2006*b* Operational hurricane intensity forecasting. *Science* **314**, 419.

BELCHER, R. J., BURGGRAF, O. R. & STEWARTSON, K. 1972 On generalized-vortex boundary layers. *J. Fluid Mech.* **52**, 753–780.

BELL, M. M. & MONTGOMERY, M. T. 2008 Observed structure, evolution, and potential intensity of category 5 Hurricane Isabel from 12 to 14 September. *Mon. Weath. Rev.* **136**, 2023–2046.

BELL, M. M., MONTGOMERY, M. T. & EMANUEL, K. A. 2012 Air–sea enthalpy and momentum exchange at major hurricane wind speeds observed during CBLAST. *J. Atmos. Sci.* **69**, 3197–3222.

BEVEN II, J. L. & LIXION, L. A. *et al.* 2008 Atlantic hurricane season of 2005. *Mon. Weath. Rev.* **136**, 1109–1173.

BLACK, P. G., PENNEY, A. B., CREASEY, R. & HARR, P. A. 2012 New eyewall dropsonde observations showing rapid intensification events in Super-Typhoon Megi (2010) and Jangmi (2008). In *Booklet of Abstracts, 66th Interdepartmental Hurricane Conference*. Silver Spring, MD, NOAA Office of the Federal Coordinator for Meteorological Services and Supporting Research. (Also, '66th IHC Presentations', www.ofcm.gov/ihc12/66IHC-Linking-File.html).

BRYAN, G. H. & ROTUNNO, R. 2009 The influence of near-surface, high-entropy air in hurricane eyes on maximum hurricane intensity. *J. Atmos. Sci.* **66**, 148–158.

BURGGRAF, O. R., STEWARTSON, K. & BELCHER, R. 1971 Boundary layer induced by a potential vortex. *Phys. Fluids* **14**, 1821–1833.

CARRIER, G. F. 1971*a* Swirling flow boundary layers. *J. Fluid Mech.* **49**, 133–144.

CARRIER, G. F. 1971*b* The intensification of hurricanes. *J. Fluid Mech.* **49**, 145–158.

CARRIER, G. F., FENDELL, F., MITCHELL, J. & BRONSTEIN, M. 1994 Self-sustaining intense vortices. *Physica* D **77**, 77–96.

CARRIER, G. F., HAMMOND, A. L. & GEORGE, O. D. 1971 A model of the mature hurricane. *J. Fluid Mech.* **47**, 145–170.

COLE, J. D. 1968 *Perturbation Methods in Applied Mathematics*. Blaisdell.

DIAMOND, H. J. 2010 Tropical cyclones: overview. In 'State of the climate in 2009'. *Bull. Am. Meteorol. Soc.* **91**, 584.

DUNION, J. P. & MARRON, C. S. 2008 A reexamination of the Jordan mean tropical sounding based on awareness of the Saharan air layer: results from 2002. *J. Clim.* **21**, 5242–5253.

ECKERT, E. R. G. & DRAKE, R. M. Jr 1962 *Analysis of Heat and Mass Transfer*, pp. 373–375. McGraw-Hill.

ELIASSEN, A. & LYSTAD, M. 1977 The Ekman layer of a circular vortex: a numerical and theoretical study. *Geophys. Norv.* **31**, 1–15.

EMANUEL, K. 2005 *Divine Wind – The History and Science of Hurricanes*, pp. 54–61, 269–274. Oxford University Press.

FENDELL, F. E. 1974 Tropical cyclones. In *Advances in Geophysics* (ed. H.E. Landsberg & J. Van Mieghan), vol. 17, pp. 1–100. Academic.

GILL, A. E. 1982 *Atmosphere-Ocean Dynamics*, pp. 326–332. Cambridge University Press.

GOLDSTEIN, S. 1960 *Lectures on Fluid Mechanics*, pp. 39–44, 63–64. Interscience.

GREENSPAN, H. P. 1968 *The Theory of Rotating Fluids*. Cambridge University Press.

HAUS, B. K., JOENG, D., DONELAN, M. A., ZHANG, J. A. & SAVELYEV, I. 2010 Relative rates of sea–air heat transfer and frictional drag in very high winds. *Geophys. Res. Lett.* **37**, L07802, doi:10.1029/2009GL042206, 5 pp.

HOLTHUIJSEN, L. H., POWELL, M. D. & PIETRZAK, J. D. 2012 Wind and waves in extreme hurricanes. *J. Geophys. Res.* **117**, C09003, doi:10.1029/2012JC007983.

HOUGHTON, J. T. 1986 *The Physics of Atmospheres*, 2nd edn. pp. 15, 19–22. Cambridge University Press.

JORDAN, C. L. 1958 Mean soundings for the West Indies area. *J. Meteorol.* **15**, 91–97.

KENDALL, J. M. Jr 1962 Experimental study of a compressible viscous vortex. In *Tech. Rep.* 32-290. Pasadena, CA, Jet Propulsion Laboratory, California Institute of Technology, 14 + vi pp.

KEPERT, J. D. 2010 Slab and height-resolving models of the tropical cyclone boundary layer. Part I. Comparing the simulations. *Q. J. R. Meteorol. Soc.* **136**, 1689–1699.

KNAFF, J. A., KOSSIN, J. P. & DEMARIA, M. 2003 Annular hurricanes. *Weath. Forecasting* **18**, 204–223.

MARKS, F. M. 2003 Hurricanes. In *Encyclopedia of Atmospheric Sciences* (ed. J.H. Holton, J.A. Curry & J.A. Pyle), pp. 942–966. Academic.

MONTGOMERY, M. T., BELL, M. M., ABERSON, S. D. & BLACK, M. L. 2006 Hurricane Isabel (2003): new insights into the physics of intense storms. Part I. Mean vortex structure and maximum intensity estimates. *Bull. Am. Meteorol. Soc.* **87**, 1335–1347.

MONTGOMERY, M. T., SMITH, R. K. & NGUYEN, S. V. 2010 Sensitivity of tropical-cyclone models to the surface drag coefficient. *Q. J. R. Meteorol. Soc.* **136**, 1945–1953.

MUSK, L. F. 1988 *Weather Systems*, pp. 118–142. Cambridge University Press.

PALMÈN, E. & NEWTON, C. W. 1969 *Atmospheric Circulation Systems – Their Structure and Physical Interpretation*, pp. 486-491, 572–577. Academic.

PEARSON, C. E. 1986 *Numerical Methods in Engineering and Science*, pp. 169–173. Van Nostrand Reinhold.

PEDLOSKY, J. 1987 *Geophysical Fluid Dynamics*, 2nd edn. pp. 179–215. Springer.

PERSING, J. & MONTGOMERY, M. T. 2003 Hurricane superintensity. *J. Atmos. Sci.* **60**, 2349–2371.

PHILLIPS, W. R. C. & KHOO, B. C. 1987 The boundary layer beneath a Rankine vortex. *Proc. R. Soc. Lond.* A **411**, 177–192.

RAPPAPORT, E. N. & FRANKLIN, J. L. *et al.* 2008 Advances and challenges at the National Hurricane Center. *Weath. Forecasting* **24**, 395–419.

RIEHL, H. 1979 *Climate and Weather in the Tropics*, pp. 446, 513–514. Academic.

SANGER, N. T. 2011 An observational study of tropical cyclone spin-up in Supertyphoon Jangmi and Hurricane Georges. Doctoral thesis, 187 pp. Monterey, CA: Naval Postgraduate School.

SMITH, R. K. & MONTGOMERY, M. T. 2008 Balanced boundary layer used in hurricane models. *Q. J. R. Meteorol. Soc.* **135**, 1385–1395.

SMITH, R. K. & MONTGOMERY, M. T. 2012 On the existence of the logarithmic surface layer in the inner core of hurricanes. *Q. J. R. Meteorol. Soc.* **138**, 1–11.

SMITH, R. K. & VOGL, S. 2008 A simple model of the hurricane boundary layer revisited. *Q. J. R. Meteorol. Soc.* **135**, 337–351.

TAYLOR, P. K. 2003 Momentum, heat, and vapour fluxes. In *Encyclopedia of Atmospheric Sciences* (ed. J. H. Holton, J. A. Curry & J. A. Pyle). pp. 93–100. Academic.

TURNER, J. S. 1966 The constraints imposed on tornado-like vortices by the top and bottom boundary conditions. *J. Fluid Mech.* **25**, 377–400.

ZHANG, J. A., BLACK, P. G., FRENCH, J. R. & DRENNAN, W. M. 2008 First direct measurements of enthalpy flux in the hurricane boundary layer: The CBLAST results. *Geophys. Res. Lett.* **35**, L14813, doi:1029/2008GL034374, 4 pp.

ZHANG, J. A. & DRENNAN, W. M. 2012 An observational study of vertical eddy diffusivity in the hurricane boundary layer. *J. Atmos. Sci* **69**, 3223–3236.

ZHANG, J. A., MARKS, F. D., MONTGOMERY, M. T. & LORSOLO, S. 2011 An estimation of turbulent characteristics in the low-level region of intense Hurricanes Allen (1980) and Hugo (1989). *Mon. Weath. Rev.* **139**, 1447–1462.